Understanding the generation and evolution of hydrophobicity of silane modified fly ash/slag based geopolymers

Cement and Concrete Composites 142 (2023) 105206

Contents lists available at ScienceDirect

Cement and Concrete Composites

journal homepage: www.elsevier.com/locate/cemconcomp

Understanding the generation and evolution of hydrophobicity of silane modified fly ash/slag based geopolymers

Yuanshan She [a], Yuxuan Chen [a,**], Lijun Li [c], Longjian Xue [c], Qingliang Yu [a,b,*]

[a] School of Civil Engineering, Wuhan University, Wuhan, 430072, PR China
[b] Department of the Built Environment, Eindhoven University of Technology, P.O. Box 513, 5600, MB, Eindhoven, the Netherlands
[c] School of Power and Mechanical Engineering, Wuhan University, Wuhan, 430072, PR China

ARTICLE INFO

Keywords:
Geopolymer
Fly ash
Blast furnace slag
Hydrophobicity
Silane
Microstructure

ABSTRACT

Silanes are widely used to enhance the corrosion resistance of cement-based materials by endowing the substrate with hydrophobicity. However, their applications in fly ash/slag based geopolymer (FSBG) are still rare. This study comprehensively investigates the hydrophobicity properties and reaction products of FSBG modified by isooctyltriethoxysilane admixture to reveal the mechanisms involved in the generation and evolution of hydrophobization effect. In spite of the verified compromise in compressive strength of modified FSBG for longer ages, the early strength at 1 day is amazingly found to slightly increase, ascribed to the heat release along with the hydrolysis of silane. The reduction of porosity is caused by the siloxane products of silane after condensation reactions and thus does not show consistencies to the decreasing compressive strength as well as the formation of hydration products. The amount of N-A-S-H gel is found to reduce more intensively compared to the C-A-S-H gel when silane is used. The evolution of contact angle on the surface of modified FSBG is dependent on the mutual effect of superficial density of silane and porosity, with the former controlled by the amount of coupling sites. The formula of contact angle evolution is proposed and can be potentially used to regulate and govern the hydrophobicity properties of FSBG, with the feasibility to be applied in other geopolymers and cement-based materials.

1. Introduction

Expected to lessen or even substitute the utilization of ordinary Portland cement (OPC), alkali-activated materials (AAMs) possess many unique advantages in reducing environmental impacts and promoted service performance [1,2]. The main raw materials in alkali-activated systems are alkaline activator and solid precursors. With the solid raw materials originating from various industrial by-products, mineral wastes and even construction and demolition wastes, alkali-activated materials make a great contribution to intractable waste treatment problem and establish a sustainable circular economy by transforming solid wastes to valuable building materials. Moreover, AAMs show excellent strength, durability and thermal stability [3], as well as reduced energy costs and carbon footprints [4]. According to the available calcium content of starting materials, alkali-activated materials can be divided into two typical binding systems: one is the high-calcium system, generating C-A-S-H type gel with a one dimensional chain structure [5]; another is the low-calcium system, also named as geopolymer, generating N-A-S-H type gel with a three-dimensional network structure [6]. Fly ash is a typical precursor for producing geopolymer, and an extra heat curing condition is generally needed during the manufacturing process [3]. To eliminate the limitation caused by the above problem and gain fast growth of strength, fly ash is often partly substituted by ground granulated blast furnace slag to introduce calcium source [5,7], consequently leading to the formation of hybrid C-(N-)A-S-H and (N,C)-A-S-H type gels as the ultimate reaction products. This hybrid system is attracting more and more attention due to its improved mechanical properties and the superior property of resistance to corrosion and elevated temperatures [8,9].

During the geopolymerization process, the Al–O–Si bonds on the surface of starting materials hydrolyze to release Si and Al monomers, both attached with four hydroxyl groups [6]. Then the monomers polymerize to form multimers and eventually the gel products.

* Corresponding author. School of Civil Engineering, Wuhan University, Wuhan, 430072, PR China.
** Corresponding author.
E-mail addresses: Yuxuan.chen@whu.edu.cn (Y. Chen), q.yu@bwk.tue.nl (Q. Yu).

https://doi.org/10.1016/j.cemconcomp.2023.105206
Received 24 March 2023; Received in revised form 30 June 2023; Accepted 5 July 2023
Available online 6 July 2023

However, there exist uncondensed hydroxyl groups on the surface of the gels, which are intimate to water and actually form the hydrophilic basis of geopolymer [1]. Combining with the inherent porous characteristic, the geopolymer products are susceptible to water invasion, which is often along with various harmful agents, constituting a great threat to the durability and restricting its wide applications [10]. There are some primary transport mechanisms accounting for the invasion process of water, including permeation, diffusion, and capillary absorption. Considering the fact that practical structural concrete always meets the unsaturated condition, capillary absorption can thus be deemed as the decisive mechanism in most situations [11]. To simplify the physical background and experimental procedures, capillary absorptions of building materials are often investigated by a unidirectional capillary absorption case. It has been discovered that the unidirectional water capillary transport behavior can be well described by so-called square-root (time) law [11]. Namely, the volume of imbibed liquid per unit area increases linearly with the square root of time, and the slope of the linear relation is defined as sorptivity. The sorptivity can reflect ingress rates of water and detrimental agents into porous materials such as cement-based materials and geopolymers, always employed as one of the most crucial indices to appraise the durability of concrete [12]. Unfortunately, geopolymers, especially containing slag as one of the precursors, have been found to exhibit greater sorptivities compared to OPC with the same W/B ratio [10,13], which can be correlated with the higher degree of network interconnectivity of pore structure [10]. To solve this problem, many attempts have been conducted to decrease the sorptivity of geopolymer matrices, such as utilization of supplementary cementitious materials [14], addition of steel fibers [15] or nano materials [16], improved curing conditions [14], and increasing fineness of precursors [17]. In spite of the beneficial effect achieved by the aforementioned methods, they are unable to change the hydrophilic nature of geopolymer matrices, which restricts the potential efficacies to a certain extent.

For this reason, the hydrophobic modification treatments can be potentially effective with the utilization of waterproof materials, such as alkyl acids and the relevant salts [10,18], organic polymers [19], silanes and siloxanes [12,20], metabolite of bacillus subtilis [21], and hydrophobic particles [22]. The modification treatments are usually classified as surface alteration and integral alteration, the latter of which has an advantage in durability but may damage the strength. Among these modification methods, the silanes are the most widely used compounds [23] due to the excellent hydrophobization effect related to their unique characteristics of functional groups [24]. The applications of silanes in the cement-based materials have been very successful in achieving lower water absorptions and sorptivities [12,25,26], however, the utilization of silanes to modify fly ash/slag based geopolymer (FSBG) is still very limited in the previous literatures. There is only one very recent study investigating the influences of polydimethylsiloxane (PDMS) on the hydrophobicity and microstructure of FSBG [27]. The addition of PDMS improved the hydrophobicity with a contact angle up to 127.64° at the concentration of 3%, and the water absorption of matrix was reduced to a great extent over 75% [27]. The other relevant researches focus on metakaolin or fly ash based geopolymer systems (MBG or FBG). Feng et al. [28] found that the uses of γ-amino propyl triethoxysilane (KH550) and γ-(2,3-epoxypropoxy) propyl trimethoxysilane (KH560) improve the hydrophobic property of MBG when a small dosage is adopted, but excessive amount of silane caused a opposite effect. The similar trends caused by silane are also observed in the hydration and porosity results. Ruan et al. [29] successfully developed waterproof MBG with a contact angle exceeding 130° by introducing PDMS, and the compressive strength was reported to firstly augment and then reduce after obtaining the maximum value. In another study [30], it was reported that the combined utilization of hydrophobic metakaolin powder and PDMS could gain better water repellence of MBG compared to single water repellent additive. The volume sorptivity and the overall amount of water imbibition are greatly decreased. Xue et al. [31] attempted to fabricate hydrophobic FBG to suppress the occurrence of efflorescence with the use of silane. The surface hydrophobicity is remarkably improved and the capillary absorption is accordingly decreased when the geopolymer samples were immersed in silane liquid transitorily. However, the mechanical properties are not influenced by the silane treatment. Obviously, the microstructure and composition of FSBG are more complicated than those of MBG and FBG [8], ascribed to the coexistence of C-A-S-H and N-A-S-H gels as the final products, which is unfortunately not fully discussed in literature [27]. It is also the case for the fresh state of FSBG considering the different raw materials between these systems. Therefore, the influence of silane can be quite different when applied in FSBG. Moreover, all these studies are not able to provide a sound explanation for the observed change of contact angle with the addition of silane, which is however highly important for its rational application to design materials with different level of hydrophobicity according to requirements. More importantly, an in-depth understanding of the hydrophobic mechanism for incorporating silane in FSBG is not available yet.

In this study, in order to figure out the impact of silane on the hydrophobicity of FSBG, a series of microstructure investigations are carried out to provide comprehensive knowledge and understanding. The hydration process and products are characterized by isothermal calorimetry, X-ray diffraction (XRD), Fourier transform infrared spectroscopy (FTIR), thermogravimetry and scanning electron microscopy (SEM) and energy dispersive X-ray (EDX). The porosity and pore structure is analyzed by gravimetry method and mercury intrusion porosimetry (MIP), respectively. Further, X-ray photoelectron spectroscopy (XPS) is applied to verify the modification by silane and detect the resultant change in chemical structure. The main objectives are to investigate the underlying hydrophobic mechanism of silane modified FSBG and elucidate the evolution of hydrophobicity with the increased concentration of silane.

2. Experiment

2.1. Materials

The solid precursors used in this study were commercial ground granulated blast furnace slag and Class F fly ash, conforming to GB/T 18046-2017 and GB/T 1596-2017 respectively. Their particle size distributions are exhibited in Fig. 1, with the d_{50} particle sizes to be 6.02 μm for slag and 17.44 μm for fly ash. The major chemical compositions analyzed by X-ray Fluorescence are shown in Table 1, with the loss on ignition (LOI) determined at 950 ± 25 °C and other material physical properties. The X-ray diffraction patterns of slag and fly ash are presented in Fig. 2. The main crystalline phases detected in fly ash are mullite, quartz and corundum. The pattern of slag has peaks of low intensity correlated with calcite and merwinite and a broad vitreous hump situated from 25° to 35° is found.

The alkaline activators were prepared by the use of sodium hydroxide flakes (analytical level, purity ≥98%), sodium silicate solution (27.3 wt% SiO_2, 8.54 wt% Na_2O and 64.16 wt% H_2O) and tap water to reach the desired moduli. The silane employed in this investigation was an aqueous emulsion of isooctyltriethoxysilane with 50 wt% available content.

2.2. Mix proportions and preparation

The employed activators had an equivalent sodium oxide (Na_2O) content of 4% by mass of the solid precursors, and three moduli of 1.5, 1.75 and 2 were adopted. In all the mixtures, the precursors were composed of 50% slag and 50% fly ash by mass, with the water to binder ratio (w/b) fixed at 0.32. Five dosages of silane varying from 0 to 2 wt% of the precursors were chosen in order to clarify its impacts on the prepared geopolymer. The detailed information of the mix design is presented in Table 2. The solid raw materials were first mixed to be

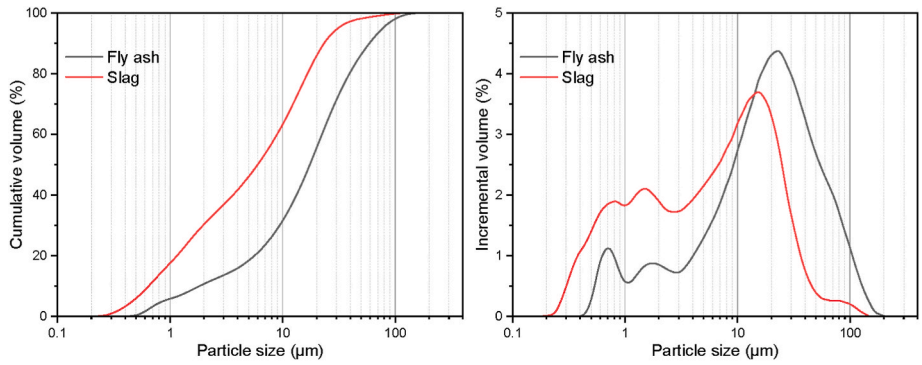

Fig. 1. The particle size distributions of precursors.

Table 1
Chemical compositions and physical properties of slag and fly ash.

Oxide (wt%)	Slag	Fly ash
SiO_2	30.15	47.44
Al_2O_3	14.88	34.70
Fe_2O_3	0.38	4.77
CaO	39.53	4.58
TiO_2	2.29	1.52
SO_3	2.48	1.28
K_2O	0.35	1.16
MgO	8.87	0.50
LOI	0.8	2.8
Specific surface area (m^2/g)	1.14	0.43
Specific density (g/cm^3)	2.90	2.55

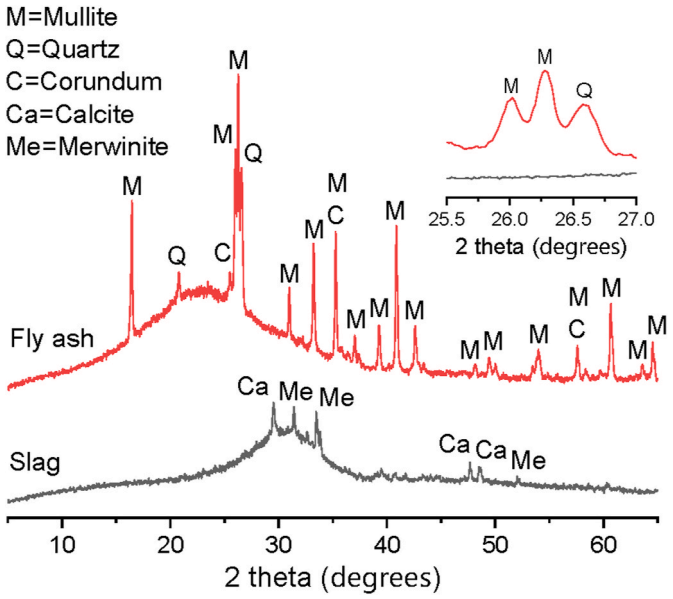

Fig. 2. XRD patterns of slag and fly ash.

Table 2
Mix design of geopolymer pastes with different concentrations of silane.

Mixture	Activator		Solid precursors		silane	w/b
	Na_2O	Modulus	Slag	Fly ash		
M*_S0	4%	1.5	50	50	0	0.32
M*_S0.5					0.5%	
M*_S1		1.75			1%	
M*_S1.5					1.5%	
M*_S2		2			2%	

* represents the activator modulus, equal to 1.5, 1.75 or 2.

homogeneous by using a FEST B20E mixer at low speed. Then the activator solution blended with silane was gradually added while stirring. The batches were mixed for 1 min with a low speed and thereupon followed by a high speed mixing for 2 min. The fresh mixtures were poured in polystyrene prismatic molds (40 mm × 40 mm × 160 mm), 50 mm three-gang molds and cylindrical molds (Φ100 mm × 50 mm) and then compacted manually before sealed by a plastic membrane. The specimens were demolded after 24 h and then cured in the climate room with a temperature stabilizing at about 20 °C and a relative humidity exceeding 95% until testing.

2.3. Experimental methods

2.3.1. Isothermal calorimetry

The isothermal calorimetry measurement was performed in a calibrated TAM-Air isothermal conduction calorimeter to investigate the hydration kinetics. The solid precursors were blended with the activators and the mixture was vibrated for 60 s externally, and then the paste was quickly poured into the ampoule and placed in the sample position.

2.3.2. X-ray diffraction

X-ray diffraction was carried out using a MiniFlex600 X-ray powder diffractometer. The Cu tube operating conditions were set as 40 kV and 15 mA, with scanning time of 0.5 s, an increment of 0.02°, and 2θ ranging from 5° to 65°.

2.3.3. Fourier transform infrared spectroscopy

The Fourier transform infrared spectroscopy measurement was executed by a Thermo Scientific Nicolet IS5 instrument with the wavelength range of 4000 to 400 cm^{-1} at a resolution of 4 cm^{-1}.

2.3.4. Thermogravimetry

Thermogravimetry was obtained using a TA SDT 650 thermal analyzer. The ground powder samples were placed in alumina crucibles and heated from 30 to 1000 °C with a heating rate of 10 °C/min in the inert atmosphere achieved by nitrogen gas flow.

2.3.5. SEM & EDX

Scanning electron microscopy (SEM) with energy dispersive X-ray (EDX) analysis was conducted using a TESCAN MIRA3 instrument. Before test, the samples were treated by epoxy resin impregnation and then polished by a grinder. The accelerating voltage was set as 20 kV and the EDX data were gained during the observation in backscattered electron (BSE) mode.

2.3.6. Mechanical strength

The compressive strength test was performed conforming to GB/T 17671 [32]. The loading rate was set as 2400 N/s and the strength was measured at 1, 7 and 28 days determined by the mean value of 3 duplicates for reducing random errors.

2.3.7. Water accessible porosity

The water accessible porosity test was conducted in accordance with ASTM C 642 [33]. The used specimens had a dimension of 50 mm × 50 mm × 50 mm. For every mix, the porosity was obtained by the average value of 4 duplicates. The saturation state of samples was achieved by the vacuum-saturated method. The single porosity result was calculated by the following equation,

$$\varphi = \frac{m_s - m_d}{m_s - m_b} \times 100 \quad (1)$$

where φ is the water accessible porosity (%), m_s is the mass of sample in saturated surface-dry condition weighed in air (g), m_d is the mass of dried sample (g) and m_b is the buoyant mass of sample weighed in water (g).

2.3.8. Mercury intrusion porosimetry

The pore size distribution of samples was obtained using a Micro-Active AutoPore V 9600 equipment. The tested samples were chosen with a particle size of around 3 mm after being crushed. The contact angle of mercury was considered as 140° when calculating the diameter of pores.

2.3.9. Water contact angle

The water contact angles of the unmodified and modified pastes at 28 days were measured in a Dataphysics OCA25 instrument. Before the test, the surfaces of specimens were polished with abrasive paper of 2000-mesh and then cleaned with water. The volume of injected water droplet was set constant as 5 μl for every measurement.

2.3.10. Water absorption test

The water absorption test of geopolymer cylinders at 28 days was performed according to ASTM C1585 [34]. The specimens were first vacuum saturated and weighed, and then these specimens were oven-dried to reach a constant mass. The side surface of each specimen was sealed by duct tape to guarantee unidirectional water transmission. Then the specimen was immersed into water for about 2 mm and the mass was recorded at the assigned time. The water absorption results are obtained by the expression,

$$I = \frac{m_t}{a \bullet d} \quad (2)$$

where I is the absorption value (mm^3/mm^2), m_t is the measured mass difference between time t and 0 (g), a is the area of the specimen contact with water (mm^2) and d is the density of water (g/mm^3).

2.3.11. X-ray photoelectron spectroscopy

X-ray photoelectron spectroscopy was accomplished using the ESCALAB 250Xi equipment with a monochromatic Al Kα X-ray source. The high resolution spectra were collected with a step size of 0.1 eV and a pass energy of 20 eV. The XPSPEAK software was utilized to analyze the spectra corrected by the adventitious hydrocarbon peak.

3. Results and discussions

3.1. Reaction process and products with and without silane

3.1.1. Reaction kinetics

The heat flow results of the mixtures with different activator moduli and silane dosages are illustrated in Fig. 3 (a) and (c). There are three typical exothermic peaks in all mixtures: The first peak can be mainly related to the immediate wetting and dissolution of the starting materials when mixed with the activator solution [5]; the second peak is attributed to the initial hydration reaction of the dissolved silicate from water glass with calcium source dissolved from slag [35]; and the third peak is due to the formation of massive reaction products [5,36]. These results are in line with previous studies for silicate activated slag [35,

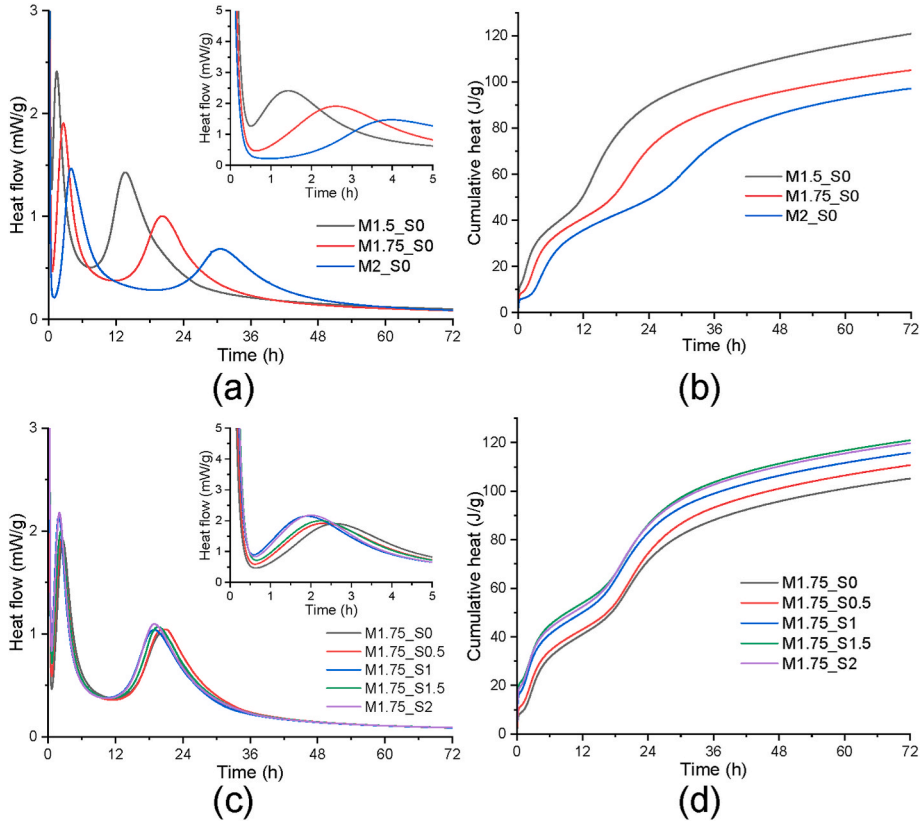

Fig. 3. The normalized heat flow (a), (c) and cumulative hydration heat (b), (d) of geopolymer pastes.

37]. It can be noticed from Fig. 3(a) that with the increase of activator modulus, the two reaction peaks shift to the right with lower intensities. The prolonged induction period also corresponds to the decreased reaction intensity because of the increasing modulus. The peak variations are mainly correlated with the decreased alkalinity and increased silica content of the activator. When activators with lower moduli are used, the resulting higher pH accelerates the dissolution rate of precursors [38], and thus the subsequent formation of reaction products. Besides, more soluble silica in the activator can generate a higher degree of polymerization of the silicate monomers [39], which impedes an immediate reaction process between silicate monomers and calcium species dissolved from precursors, consequently resulting in an extended reaction time.

Fig. 3(c) shows heat evolution curves with different silane dosages from 0 to 2%. It is obvious that with the addition of silane, the intensities of the last two heat output peak are slightly increased and the occurrence times of the peaks are mildly reduced as well as the induction period, with the outline of curves keeping unchanged. These results reveal that the inclusion of silane accelerates the hydration process during the first 72 h without influencing the underlying hydration reaction mechanisms. The hydrolysis of silane catalyzed by hydroxyl ions in the activator may account for the accelerated hydration process, which is reported to occur with the release of heat [40]. Moreover, a certain amount of water can be consumed to substitute ethoxy groups on the Si atoms in the hydrolysis process, leading to an increase in the alkalinity to certain extent. Another reason is the formation of hydrogen bond between intermediate hydrolysis products of silane and precursor grains or reaction products [41], which is believed to be an exothermic process [42]. The above-mentioned explanations can be confirmed by a relevant research [43] in which the setting time was prolonged when the used silane endured a pre-hydrolysis process. However, excessive silane could cause a relatively lower hydration intensity, although it may be still higher than the reference sample. This could be explained as the sorption effect of silane molecules on the surface of precursor grains, which has been verified in the cement systems [44]. The adsorbed silane molecules form a hydrophobic film around starting materials, hindering the free contact with water and basic ions, and thus the hydration process is partly suppressed. This similar inhibiting effect can be found in previous study in which calcium stearate is used to modify alkali-activated slag [10]. It is concluded that the combined effect of the mentioned mechanisms ultimately dominates the hydration reaction at an early stage.

Fig. 3(b) and (d) show the cumulative heat output of different geopolymer pastes. It is indicated that a higher activator modulus leads to a stronger cumulative heat release. The similar trend can be found with the addition of silane. The overall heat output during the first 72 h is believed to be the indication of the reaction degree, and hence the evolution of mechanical strength. In fact, the presented results here could be well correlated with the mechanical strength data in subsequent section, which will be further investigated.

3.1.2. XRD analysis

The XRD patterns of paste mixtures after 28 days curing are illustrated in Fig. 4. In all the mixtures, mullite ($Al_6Si_2O_{13}$), quartz (SiO_2) and calcite ($CaCO_3$) are found as residual crystalline phases present in the unreacted fly ash and slag powders. These crystals are considered as inert constituents without participation in the alkali activation process [45]. Although some variability in quartz peak intensity can be observed from the presented patterns, it should be ascribed to the variation of particle size of fly ash in the test samples, rather than implication of chemical reaction [46].

The broad hump in the paste mixes located from around 20 to 40° reflects the amorphous structure of aluminosilicate gel [5,9]. In the meantime, a peak superimposed on the amorphous hump can be observed near 29.5°. This peak is ascribed to the poorly crystalline calcium silicate hydrate (C-S-H) type phase ($1.5CaO{\cdot}SiO_2{\bullet}xH_2O$) which is in line with previous literatures where C-S-H gel existed as main hydration product in slag-rich alkali activated systems [47]. Due to the incorporation of aluminum or sodium, the C–A–S–H or C–N–A–S–H type gels may be formed. The peak could partially correspond to calcite originating from remainder of slag or carbonation of reaction product as well, the presence of which is also detected by thermogravimetric analysis to be discussed in following section. The intensities of C-S-H phase peaks and broad amorphous hump are found to decrease with larger silane dosages, implying that hydration degree and microstructure development are slightly inhibited by adding silane. This can be also reflected by compressive strength results, as presented in Section 3.2. As a class of anionic clays, hydrotalcite is formed with sufficient quantities of magnesium and aluminum in highly alkaline system (pH > 9) [48], possessing a brucite-type layer structure and containing carbonate ions as well as water molecules in the interlayer region [49]. It has been widely reported as one of the hydration products in alkali activated slag or slag/fly ash blends [9,45]. However, the hydrotalcite phase is undetected in all mixtures. This is mainly because hydrotalcite is finely intermixed with the C-S-H gel and thus could not be distinguished by XRD [50]. The presence of hydrotalcite phase is to be revealed through the thermogravimetric analysis results presented below. It should be noted that any new crystalline phase is not induced by the addition of silane, indicating that main skeleton structure of geopolymer is actually unaffected, although some relevant chemical reactions may take place.

3.1.3. FTIR analysis

The infrared spectra of raw fly ash and slag are presented in Fig. 5(a). The tiny peaks centered at about 3450 cm^{-1} and 1637 cm^{-1} are correlated with the stretching and bending vibration from water respectively.

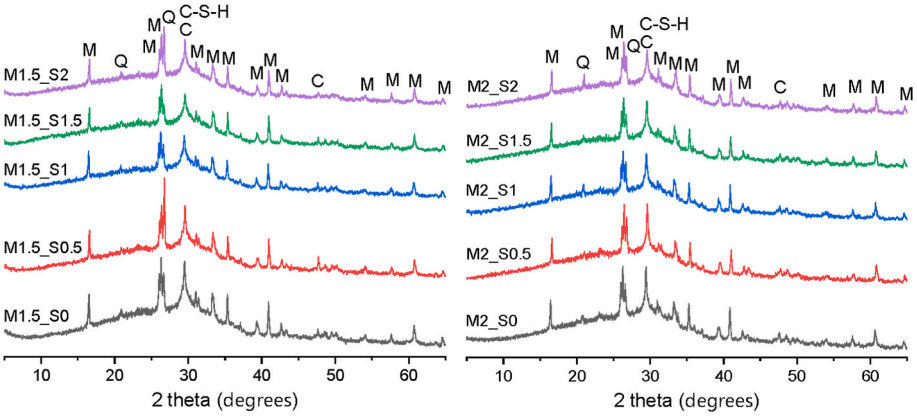

Fig. 4. XRD patterns of geopolymer pastes. (Left) Modulus 1.5. (Right) Modulus 2. (C-S-H - calcium silicate hydrate, Q - quartz, M – mullite, C - calcite).

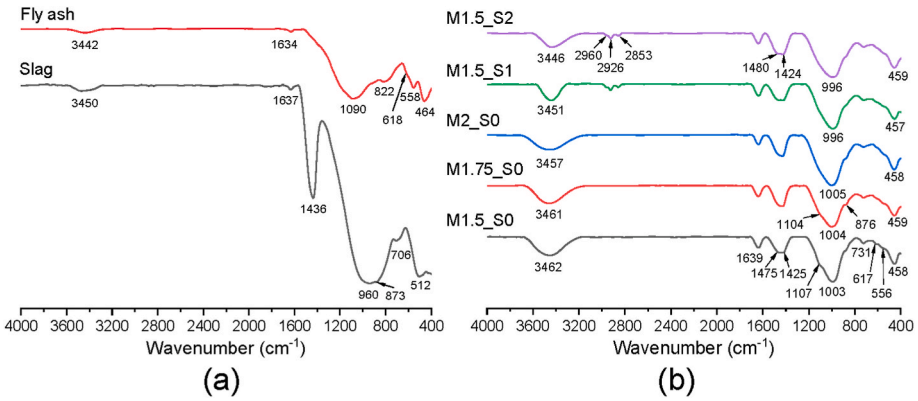

Fig. 5. FTIR spectra of (a) solid precursors and (b) geopolymer mixtures.

The absorption peak located from 1250 to 900 cm^{-1} corresponds to asymmetric stretching of Si-O-T bonds, where T represents silicon or aluminium tetrahedron. It can be observed that the position of the peak of slag shifts to a smaller wavenumber compared to that of fly ash, which is expectable considering the presence of calcium network modifiers breaking down the Si-O-T bonds in the glassy structure. For fly ash, the aluminum tetrahedron and aluminum hexahedron vibrations appears at 822 and 558 cm^{-1} due to mullite [51]. The peak shoulder at 618 cm^{-1} is ascribed to the presence of corundum (a crystalline form of aluminium oxide (Al_2O_3)) [52]. The absorption peak related to the vibration from quartz is detected at 464 cm^{-1}. As for slag, the bands at 1436 cm^{-1}, 873 cm^{-1}, and 706 cm^{-1} indicate the presence of calcite with different vibration modes, including asymmetric stretching vibrations for 1436 cm^{-1}, out-of-plane deformation vibrations for 873 cm^{-1}, and in-plane deformation vibrations for 706 cm^{-1} [53]. The absorption peak appearing at 512 cm^{-1} corresponds to the vibration modes of merwinite [54]. These results are in line with what have been obtained by XRD (Fig. 2).

The infrared spectra of geopolymer paste mixtures cured for 28 days are shown in Fig. 5(b). The broad band between 3200 and 3600 cm^{-1} is related to the hydroxyl groups in the hydrated products, regarded as an indicator of the reaction degree [48]. According to the intensities of the corresponding peaks, it can be speculated that the extent of hydration of the pastes reduces with the modulus or silane dosage, which corresponds to the XRD data as elaborated above. In the mixtures with addition of silane, new absorption bands appearing at 2960 cm^{-1}, 2926 cm^{-1} and 2853 cm^{-1} are attributed to the stretching vibration modes of methyl and methylene groups [31], which are believed to originate from the alkyl functional groups in the silane, revealing the implemented bonding between silane molecules and surface of hydration products. In the paste mixtures, the wide peak at 1250 to 900 cm^{-1} assigned to the Si-O-T asymmetric stretching vibration is mainly determined by the hydration products, with slight effect caused by the remnant unreacted raw materials. Actually, the traces of unreacted components of the fly ash can be still identified in M1.5_S0 and M1.75_S0, as a shoulder appears at about 1100 cm^{-1}. For mixtures without silane, the position of Si-O-T peaks slightly shift to higher frequencies as the modulus increases. The variation of band position is usually related to different Al/Si and/or Ca/Si ratio in the C-(N-)A-S-H gel [55], or the formation of hydration product with higher degree of polymerization and/or cross-linking of aluminosilicate chains [56]. With the increase of activator modulus, the quantity of available silica within the system augments, as well as the silicon proportion in the ultimate hydration products [56]. Therefore, it is the changes of Al/Si and/or Ca/Si that result in variation in wavenumber of the major peak. In regard to the mixtures with a modulus of 1.5, a reduction in wavenumber of the broad absorption peak is found with the addition of silane. Since there are no aluminum and calcium sources introduced by silane, the explanation should be different. In the previous section, it has been confirmed that the hydration process is slightly suppressed by introducing silane. According to the current results, the formation of N-A-S-H gels is believed to endure more intense retardation effect than that of C-A-S-H gels, with the former having a higher wavenumber [56]. Another peak related to the hydration product is situated at 731 cm^{-1}, correlated with the symmetric stretching of Si-O-Si bonds [57]. The presence of hydrotalcite by-products are detected in all the paste mixtures, with deformation vibration of Mg-O and Al-O bonds at 617 cm^{-1} [55]. This suggested again that the inclusion of silane does not influence the hydration products of the activation of slag/fly ash blends. Moreover, it is noteworthy that a new calcium carbonate polymorph aragonite appears in the spectra, with the peak at around 1480 cm^{-1} corresponding to the asymmetric stretching of O-C-O bonds in carbonate groups [58]. This new phase is deemed to be one carbonated product of the geopolymeric gel, indicating that the samples have experienced a slight degree of carbonation.

3.1.4. Thermogravimetric analysis

Differential thermogravimetric (DTG) results of geopolymer pastes at 28 days are shown in Fig. 6. The observed major endothermic peak of all the mixtures is centered at around 100 °C, which could be partly accounted for by evaporation of free or physically bound water. As for the main hydration products, the C-S-H type gel has a decomposition temperature ranging from 20 to 220 °C in cement and alkali-activated slag (AAS) systems [59], and the N-A-S-H type gel is reported to dehydrate at approximately 100 °C [47]. The water loss of the two gel products could make a primary contribution to the major peak. The second peak located at about 350 °C is correlated with the decomposition of hydrotalcite phase releasing structural water and carbon dioxide. This is consistent with the infrared spectra results previously presented, also in line with those reported for AAS or alkali-activated slag/fly ash (AASF) [56,59]. The mass loss located at around 480 °C is hardly seen in the mixes without silane but quite apparent when silane is added, especially for a higher amount. This peak corresponds to the decomposition of the organic groups of silane, as previous literatures demonstrated [60]. The calcium carbonate phase dissociation is first observed due to the mass loss from 630 °C to 680 °C in all the samples, and noticed again from the peak approaching 820 °C, which is associated with the decomposition of calcite. Compared to aragonite, calcite is deemed to decompose at a higher temperature, because calcite is the most thermally stable form among the calcium carbonate polymorphs [61]. The characteristic peaks of portlandite are undetected in paste mixtures, consistent with preceding XRD and FTIR results. Considering the abundance of silica and alumina in the blend system, it is understandable because the C-A-S-H gel is more likely to form rather than portlandite in this situation [55].

According to the dissociation process of product gels over temperature as aforementioned, the total amount of gels could be represented by

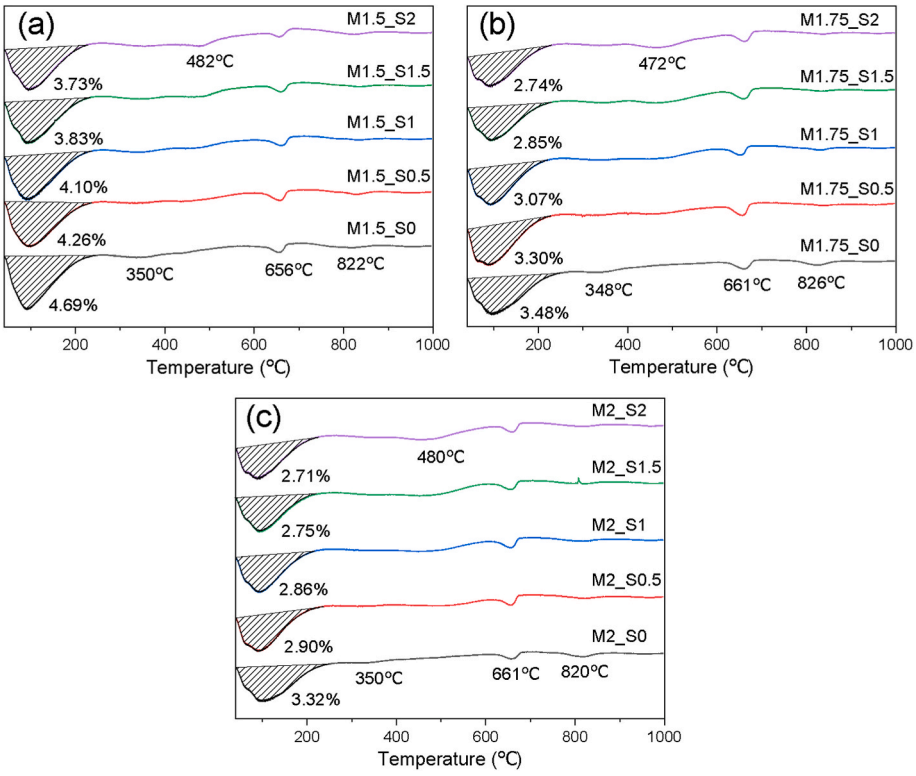

Fig. 6. Differential thermogravimetry (DTG) curves of geopolymer pastes with (a) modulus 1.5, (b) modulus 1.75 and (c) modulus 2.

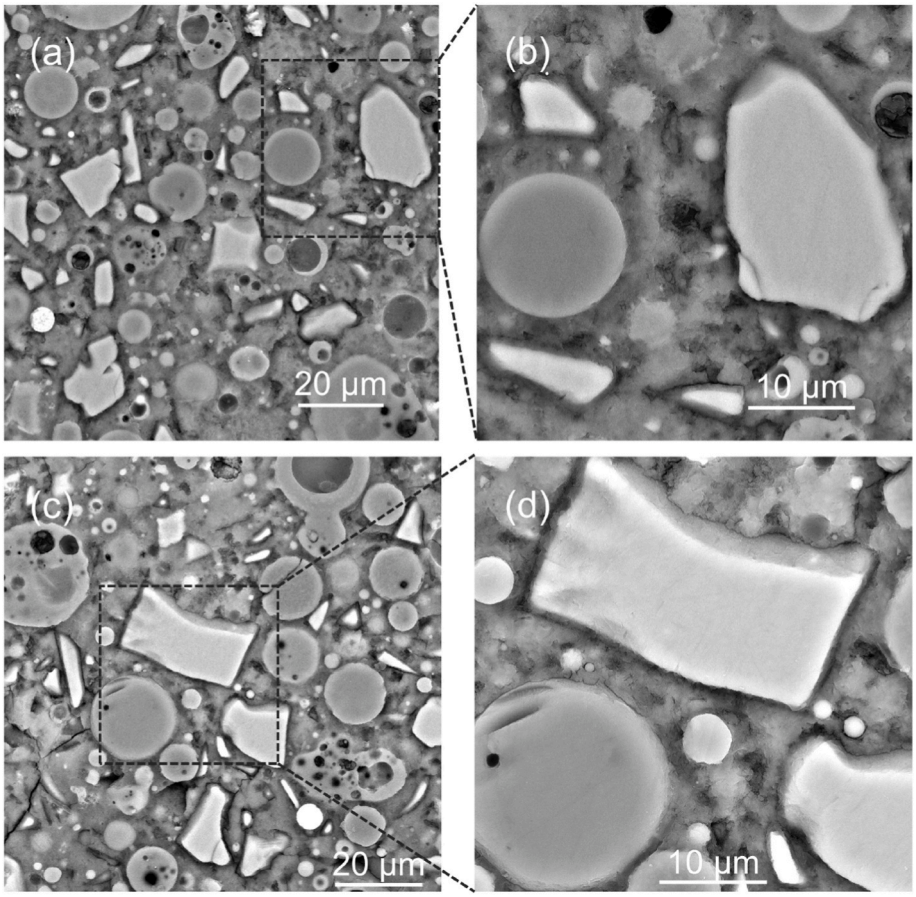

Fig. 7. BSE images of pastes of modulus 1.5 with no silane (a), (b) and a 2% silane dosage (c), (d) at 28 days.

the mass loss of the peak between 40 and 240 °C centered at about 100 °C. The activator modulus makes a great contribution to the formation of hydration gels, samples with higher modulus possessing less mass loss for the identical silane dosage. Taking the mixes without silane as an example, as the modulus increases from 1.5 to 2, the corresponding mass loss decreases from 4.69% to 3.32%. This is in agreement with the heat flow data as previously discussed. The addition of silane seems to hinder the formation of reaction products to a certain extent. For the samples with a modulus of 1.5, the mass loss is reduced from 4.69% to 3.73% when silane is introduced at a content of 2%. This trend is the same as what has been reflected by preceding XRD and FTIR data.

3.1.5. SEM & EDX analysis

Back Scattered electron (BSE) images of paste mixtures at 28 days are illustrated in Fig. 7. The unreacted fly ash particles can be identified to be equally distributed in the matrices, with spherical shape rims and a light grey color. The angular shaped particles showing a brighter grey color than fly ash correspond to slag, which is related to the different chemical compositions, specifically the abundance of calcium in slag [9]. The gel phase is well-distributed in the whole area, showing a darker grey color compared to the fly ash. The black regions are ascribed to the hollow fly ash beads or the pores. For the paste of modulus 1.5 with no silane addition, the gel phase is seen to closely surround the fly ash particle. However, when 2% silane is introduced, there is apparent interspace between the gel and the particle, forming visible microcrack. It can be observed more easily in the magnified images Fig. 7(b) and (d). This could be attributed to the formed hydrophobic film mentioned in Section 3.1.1. The added silane can be adsorbed onto the surface of a portion of precursor particles, impeding the free contact to the alkaline solution and slowing the hydration kinetics. Therefore, this surface might become the weak area in the matrix. Considering the inevitable shrinkage-induced microcracks, which originate from the self-desiccation along with the production of C-A-S-H and N-A-S-H gels or the shrinkage level discrepancy between the two products [62], the resultant crack propagation could happen more easily in the vicinity of the surface, as demonstrated in Fig. 7(c).

EDX data of different paste mixtures are also gathered so that the constitution of the hydration products and the possible variation can be recognized. Those points chosen to be measured are carefully decided with adequate distance away from the remnant grains of starting materials, in order to only provide the information of the binder region as much as possible. The CaO-Al_2O_3-SiO_2 ternary diagrams obtained from normalization of the content of the three elements are presented in Fig. 8. It can be seen that the EDX results are attributed to the C-A-S-H type gel [9,56] or the (N, C)-A-S-H type gel [55,63]. The solid and dotted black elliptic lines are drawn to indicate the C-A-S-H gel and (N, C)-A-S-H gel respectively. The coexistence of the two gels is well in agreement with the previous studies for slag/fly ash blend system [55, 64]. From Fig. 8(a), the compatibility state of the gels is not influenced by the change of modulus generally, which demonstrates that only the production of hydration products is suppressed when the modulus increases. The impact of silane over the constitution of gel products is presented in Fig. 8(b). It seems that the proportion of C-A-S-H gel within the whole gel products has an increasing trend as the dosage of silane increases. This could be a proof of the deduction proposed in the FTIR analysis that the formation of N-A-S-H type gel is inhibited more intensely compared to the C-A-S-H type gel. The reason might be that the silane has a better affinity to the surface of fly ash during the adsorption process than that of slag, which will be further discussed in Section 4.1.

3.2. Mechanical strength

The compressive strength of geopolymer pastes with different silane dosages and moduli are illustrated in Fig. 9. Regardless of the alkaline activators utilized, it seems that the influence of silane content on compressive strength is dependent upon the hydration age. More specifically, as the concentration of silane increases, the compressive strength increases firstly and then decreases when passing the peak for the age of 1 day. Nonetheless, at 7 and 28 days, the mechanical property is monotonously reduced with the increased silane dosage. The similar results can be seen elsewhere [65]. This phenomenon can be closely related to the influence of silane over the hydration process. According to the isothermal calorimetry results, the addition of silane could speed up the reaction and therefore causes an increased formation of hydration products at early age, enhancing the compressive strength to a certain extent. However, excessive silane is not favorable for the development of mechanical strength, because the retardation effect begins to be predominant compared to the acceleration effect. For ages of 7 or 28 days, the promotion provided by the silane is basically ignorable, so the generation of reaction products is mainly restrained and the compressive strength is consequently reduced. This is consistent with the thermogravimetric data previously presented. Furthermore, the influence caused by activator modulus on mechanical strength is noteworthy. When the modulus changes from 1.5 to 2, the compressive strength experiences a monotonic decrease. The activators used in current study are composed of sodium hydroxide and water glass, which are able to provide extra silica to the hydration reaction. Considering that the initial dissolution of Al from precursors is faster compared to that of Si [6], the additional silica can react with the dissolved aluminum to produce aluminosilicate gel. It is the reason why using activator composed of water glass and sodium hydroxide can achieve better strength mechanical property than using sodium hydroxide solely [6]. However, as the modulus exceeds an optimal value, the excessive amount of silica and the insufficient basicity can hinder the dissolution of precursors as well as the subsequent polymerization reaction [5], causing a decrease in mechanical property. This is exactly the trend shown in the present mechanical strength

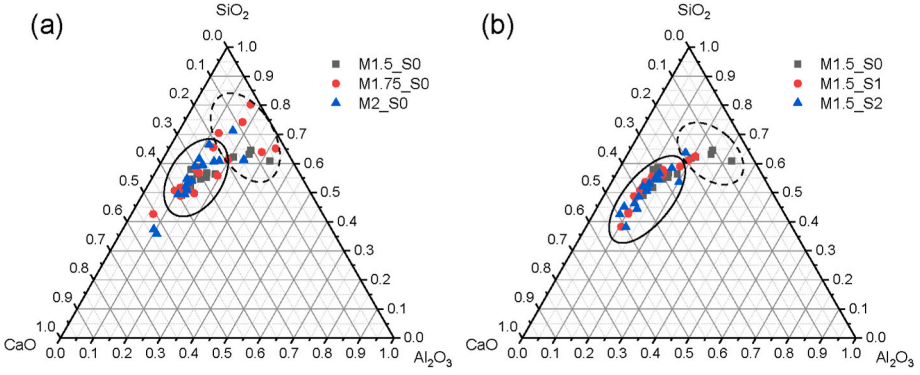

Fig. 8. Ternary diagrams of EDX results for geopolymer pastes. Data encircled by the solid black elliptic line are correlated with the C-A-S-H type gels and dotted black elliptic line indicates the (N, C)-A-S-H type gels.

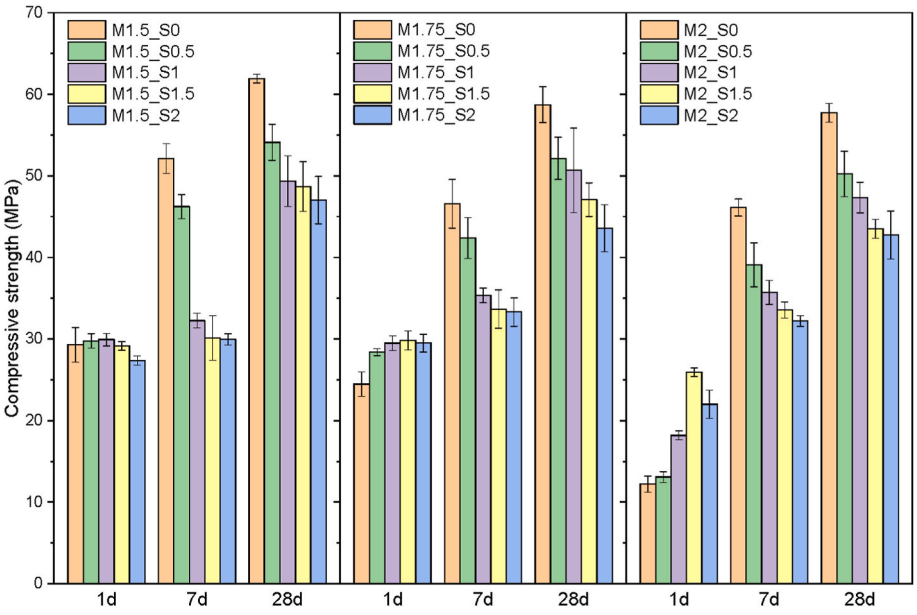

Fig. 9. Compressive strength of geopolymer samples at different ages.

results.

3.3. Pore structure analysis

3.3.1. Permeable porosity

The water-accessible porosities of the geopolymer pastes at 28 days are shown in Table 3. Regardless of the concentration of silane, the porosity increases as the modulus increases, consistent with the FTIR, thermogravimetric, and mechanical strength results. Moreover, with the silane dosage increasing, the permeable porosity basically shows a downward trend. However, this is not in line with the results reported for slag/fly ash blend system [56], where the porosity is mainly influenced by the amount of hydration product, and less formation of hydration product means larger porosity of the matrices. This difference could be attributed to the addition of silane in our study, which may influence the porosity results due to the shrinkage reduction effect [66]. Since the geopolymer matrices are modified to be less hydrophilic by silane, the menisci formed in the pores show lower curvatures and the corresponding negative capillary pressures will be accordingly decreased, which are widely accepted as the main source of shrinkage [62,66]. Consequently, it can be reasonably speculated that the shrinkage of the geopolymer matrix is reduced to a certain degree. And the measured water-accessible porosity is here observed to decrease as the shrinkage induced microcracks are suppressed. Due to the fact that geopolymer is thought to be susceptible to shrinkage problem, this effect could actually make a considerable difference.

3.3.2. MIP analysis

The pore size distribution of geopolymer mixtures detected using MIP at 28 days is illustrated in Fig. 10. Fig. 10(a) and (b) present the influence of modulus on the cumulative and differential pore volume respectively. It is found that with a higher modulus, the total mercury-intruded volume is increased, which indicates a higher porosity. This is in accordance with the water permeable porosity data as previously discussed. Three moduli exhibit similar differential pore volume curves, which means that the characteristic pore network structure of the geopolymer matrices is not affected generally. The critical pore diameters of the three mixtures are close as well, located at about 20–30 nm. If considering the pores less than 10 nm, the differential curve of modulus 1.5 shows a higher value. Given that the characteristic size of gel pores is also in this range [67], it might indicate a larger amount of the production of reaction products, which is consistent with the thermogravimetric results. A similar phenomenon can be found in the literature [8]. The effect of silane over the pore size distribution of paste mixes can be different. Fig. 10(c) shows that the cumulative pore volume firstly increases and thereupon decreases basically with the increased silane dosage. Firstly, the formation of gel products could be suppressed when silane is added, thus leading to a higher porosity. However, the introduced silane can adsorb on and ultimately be bound to the surface of the matrix of geopolymer, thus occupying a certain amount of space and reducing the porosity in the macro scale. When the dosage of silane reaches a greater value, this effect becomes predominant and the total porosity decreases. Similar result has also been found in previous study in silica gels [68]. In Fig. 10(d), the relative proportion of pores less than 10 nm and that between 10 and 100 nm is found to increase as the silane dosage increases. This could be mainly correlated with the porous structure formed by the condensation between the hydrolysis products of silane [28]. In the porous structure, different silane molecules are interconnected by Si-O-Si bonds, having a silica gel-like network. Further, the silica gels were reported to possess a refined pore structure, and the majority of pores are less than 10 nm [68]. Therefore, it is believed that the pore network structure of pastes is improved by the siloxane as the ultimate products of silane, rather than the optimization of the true gel skeleton. This might explain why the measured porosity results are not really in accordance with the mechanical strength data.

Table 3
Permeable porosity of samples with different silane dosages and moduli. (Standard errors in brackets).

Porosity (%)	Silane dosages (%)				
	0	0.5	1	1.5	2
Modulus 1.5	25.9 (0.63)	23.7 (0.48)	23.4 (0.56)	23.1 (0.75)	22.2 (1.05)
Modulus 1.75	28.8 (0.36)	28.3 (0.36)	28.6 (0.97)	28.4 (0.48)	28.0 (0.40)
Modulus 2	29.3 (0.71)	28.7 (0.47)	28.9 (0.42)	28.6 (0.71)	28.4 (0.63)

3.4. Contact angle

To figure out the hydrophobicity nature of geopolymer matrices with and without the addition of silane, the contact angle test was performed

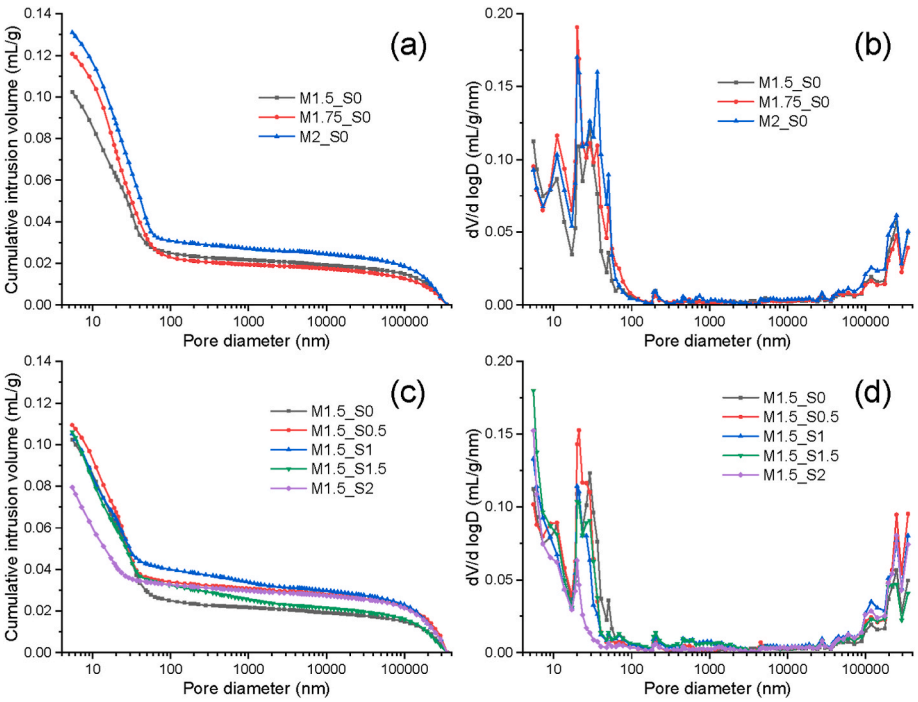

Fig. 10. Pore size distribution of geopolymer pastes at 28 days.

to all the paste samples at 28 days. It should be mentioned that the measured data are the so-called apparent contact angle instead of the intrinsic value, on account of the abundance of pore structure ranging from nanometer to micrometer level on the surface of paste. Nevertheless, the acquired results are able to indicate the change of hydrophilicity characteristic of the paste surface [12]. The contact angle results with different moduli and silane content are shown in Fig. 11. Regardless of the activator used, the modified paste always possesses a higher contact angle compared to the mixture without silane. The maximal contact angle of 118.1° is observed with the modulus of 1.5 at a 1% silane dosage. These results demonstrate the significant hydrophobization effect caused by the silane. The contact angle is noticed to increase as the modulus increases from 1.5 to 2 for the mixes without silane. This could be related to the porosity variation discussed above, which is believed to affect the contact angle to a certain extent [12,69]. The contact angles have a different variation trend in terms of the modulus. The angle is observed to firstly increase and then decrease as the silane content increases for the modulus of 1.5, but the values keep increasing with the other two higher moduli. Obviously, this difference will influence the application strategy of silane in the situation where waterproof requirement is to be satisfied. This phenomenon will be further discussed in Section 4.2.

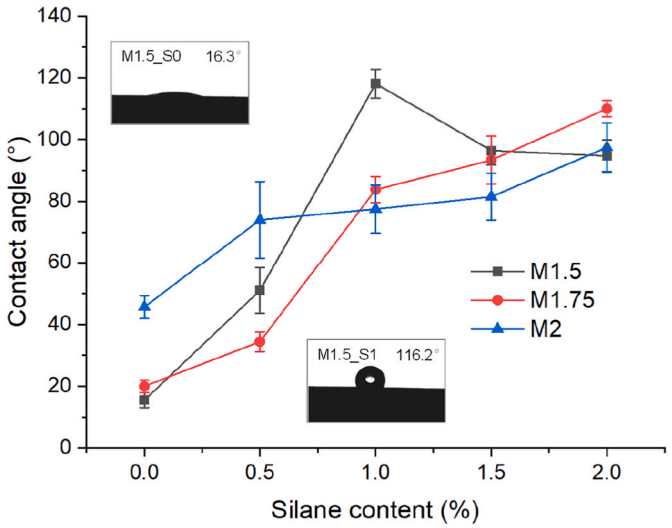

Fig. 11. Contact angles of water droplets on the geopolymer pastes.

3.5. Water absorption process

The water absorption results of all the mixtures are shown in Fig. 12. It is found that the water absorption of all mixtures experience a linear growth stage for the first 30 min, which corresponds to the previous studies [10,11]. However, the slope of curves has a declining trend with the elapse of time, indicating a discrepancy with the classical square root of time law. This could be related to the swelling of the gel products [11], causing less interspace in the matrix for the transmission of water and therefore lessening the rate of absorption.

Compared to the mixes modified by silane, the samples without silane have a much higher water sorptivity, and their plateaus appear at a significantly earlier time. This notable difference verifies again the hydrophobic effect from the introduced silane. With the increasing silane content, the amount and rate of water absorption of the samples are both reduced, which could be first associated with the reduced porosity. In the meantime, it should be mentioned that the capillary absorption of water into the geopolymer matrices is determined by the porous network of the matrices and the characteristics of water consisting of surface energy, dynamic viscosity along with contact angle in the three phase interface [12]. Generally, surface energy and dynamic viscosity of water can be considered as constants, so their effects on the water absorption are ignorable. Therefore, the increasing contact angle should be the other reason for the slower water absorption. The case is different for the samples with a modulus 1.5. Here the lowest sorptivity is found at a dosage of 1%, and the sorptivity is found to increase as the dosage reach 1.5%, but deceases again with the dosage increasing to 2%. It is consistent with the contact angle results of modulus 1.5 for the dosage less than 1.5%. This is reasonable considering the fact that the contact angle only has a 1.8° reduction when the content increases from 1.5 to 2%, with the porosity experiencing a considerable decline on the

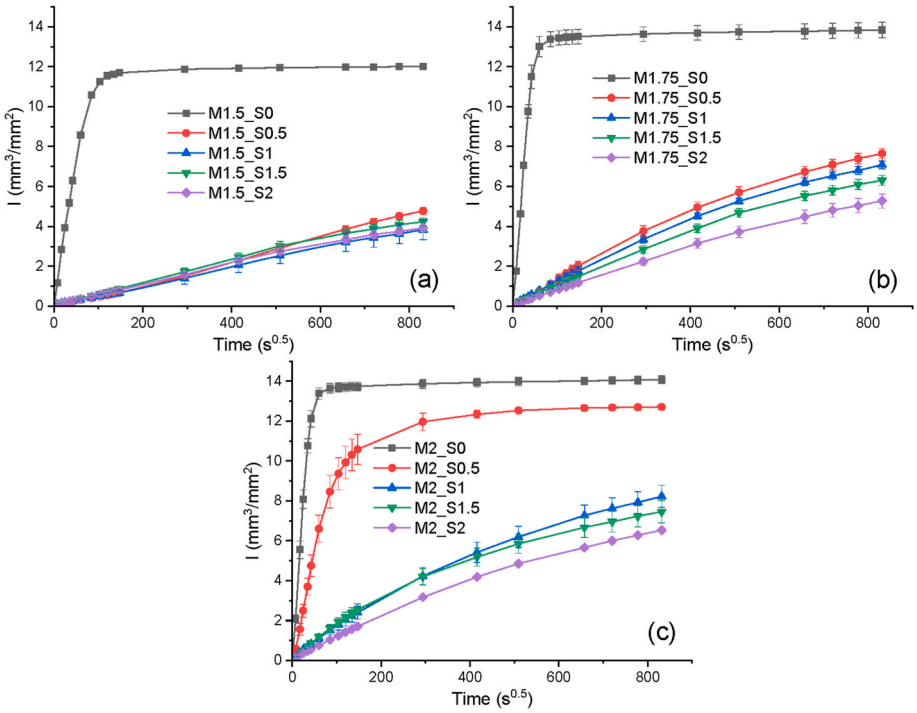

Fig. 12. Water absorption curves of pastes with the moduli 1.5 (a), 1.75 (b) and 2 (c).

contrary. For the influence of the activator used, it is observed that the water sorptivity is increasing as the modulus enhances, which can be mainly ascribed to the porosity variation discussed in the pore structure analysis.

3.6. XPS analysis

The XPS survey spectra of geopolymer pastes at 28 days are shown in Fig. 13. The XPS survey scan of all the samples are seen to possess the same photoelectron peaks and Auger lines, which are attributed to the elements of O, Na, Ca, Mg, Si and C [70,71]. It is clear that the intensity of C 1s peak is increased with the silane content increasing from 0 to 2%, reflecting the incorporation of silane into the geopolymeric substrates. The C 1s spectra of samples with different silane content are illustrated in Fig. 14(a), (b) and (c). For the mixture without the addition of silane,

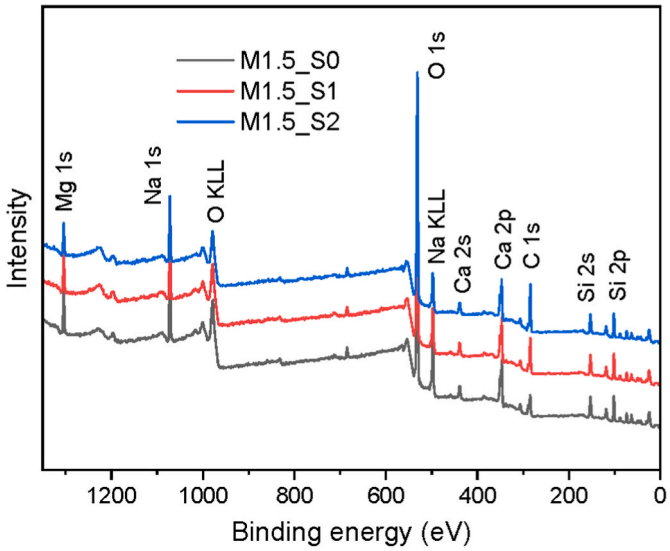

Fig. 13. XPS survey spectra (wide range) of geopolymer mixtures.

the presence of three carbon environments seen in the spectrum is related to the C-C and C-H (284.72 eV) groups, C-O (285.87 eV) groups and the species of $CaCO_3$ (289.33 eV), with the organo-functional groups originating from the adventitious carbon [72]. The peak of calcium carbonate can be associated with the remnant crystalline phase of precursor grains or the carbonization product when exposed to the atmosphere, which is in good accordance with previous XRD, FTIR and thermogravimetric results. A different chemical state of carbon appears for the samples modified by silane, identified as the C-Si (283.6 eV) groups stemming from the silane molecules. Moreover, the content of C-Si bonds is found to increase when a larger amount of silane is used, as well as that of the C-C and C-H bonds, over the basis of the $CaCO_3$ content. This indicates that with the increase of the silane dosage, more silane molecules are combined on the surface of geopolymer matrices. The O 1s spectra of the paste samples for age of 28 days are presented in Fig. 14(d), (e) and (f). All the spectra exhibit three chemical states ascribed to the Si-OH and C-O (532.47 eV) groups, the Si-O-T groups and $CaCO_3$ (531.52 eV) and the Si-O-Na (530.16 eV) groups. The existence of silanol bonds can be correlated with the uncondensed Si-OH groups on the surface of the gel products and that of the hydrolysis products of silane [73]. The Si-O-T groups correspond to the silicon-aluminum framework of the hydration products and the Si-O-Na bonds can be regarded as an indicator of the presence of non-bridging oxygen at the extremities of gel chains [74]. It is observed that with the increasing concentration of silane, the content of Si-O-T groups is reduced, and meanwhile the percentage of Si-OH and Si-O-Na bonds are found to increase. The increase of Si-OH bonds could be associated with the introduction of silane, the hydrolysis product of which has been demonstrated to reserve a portion of Si-OH groups after the condensation process [73]. The changes of the content of Si-O-T and Si-O-Na groups together point to the size of geopolymer particles [74]. In fact, the average chain length of the gel products has been found to decrease when the hydration process is delayed [75,76]. This result is well in line with the thermogravimetric results previously presented, showing that silane has a retardation effect on the geopolymerization in the long term.

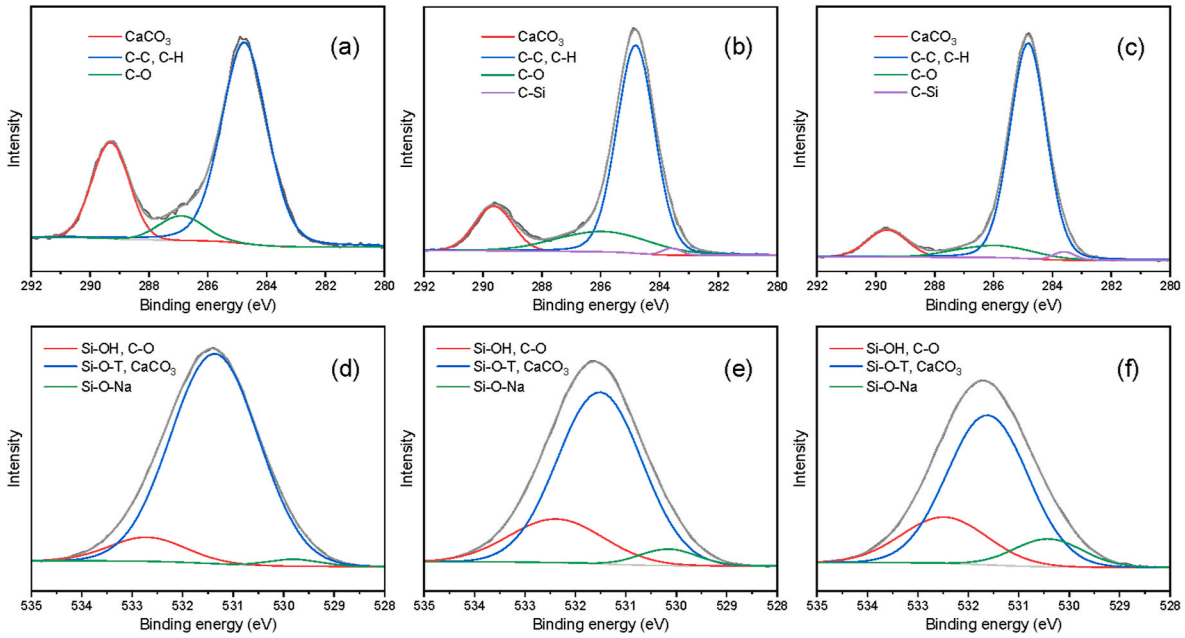

Fig. 14. C 1s spectra (narrow range) of samples of modulus 1.5 with silane dosages at 0 (a), 1% (b) and 2% (c) and O 1s spectra (narrow range) of samples of modulus 1.5 with silane dosages at 0 (d), 1% (e) and 2% (f).

4. Discussions

4.1. Hydrophobic modification mechanism of silane admixture

When silane is introduced into the geopolymer system as an additive, it is always accompanied with a series of chemical reactions and physical processes including the hydrolysis and condensation of silane and the subsequent adsorption action, etc. This could be notably different from the situation where the silane is utilized to fabricate external hydrophobic coatings [23], due to the high maturity of gel products already having a stable skeleton structure [31]. For the sake of figuring out the comprehensive effect of silane admixture on the FSBG matrices, the states of silane after being mixed with the other raw material are carefully studied considering their interactions. The diagrammatic

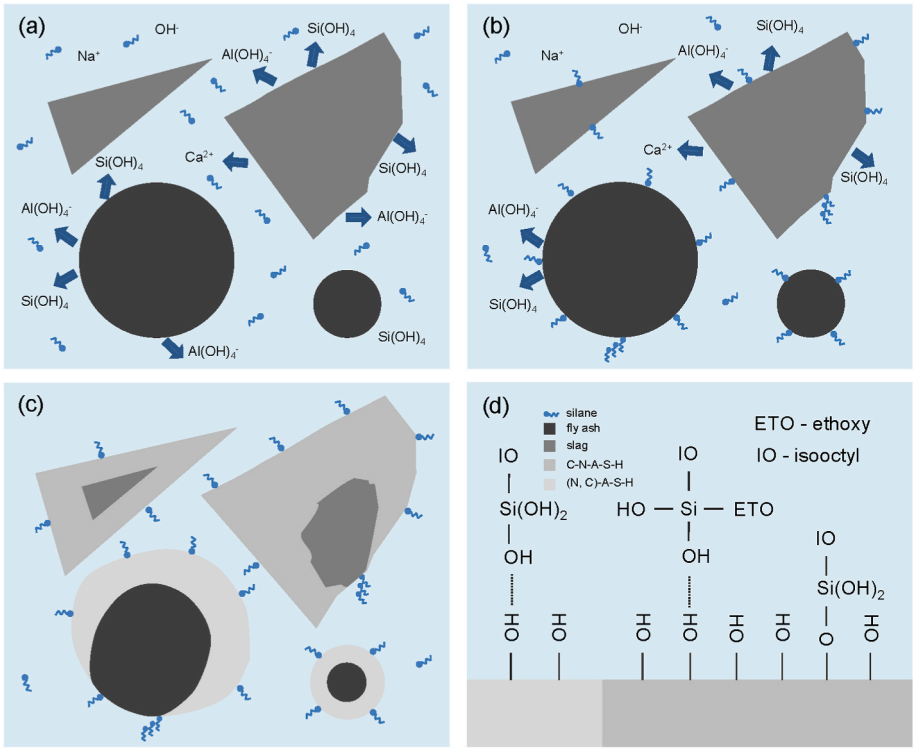

Fig. 15. The hydrophobic mechanism of silane modified geopolymer paste. (a) The hydrolysis of silane and the hydration reaction occurring in the first few hours; (b) and (c) the adsorption of the silane hydrolyzed products onto the surface of precursors and hydration products; (d) the bonding of silane to the silanol groups of the gel products.

representation of modification mechanism with the applied silane is illustrated in Fig. 15 to better understand the obtained results in this research.

The original condition here considered is a uniformly distributed system after the mixing process, where the oil-like silane can behave as a lubricant to achieve better dispersion [29]. Within the first several hours, the silane begins to quickly hydrolyze due to the catalysis action under the highly alkaline environment, with the substitution of hydroxyl for alkoxyl. In the same time, the first stage of hydration is occurring attributed to the availability of Ca^{2+} releasing from the surface of slag and the $Si(OH)_4$ existing in the activator solution. Due to the heat release along with the hydrolysis reaction, the formation of gel products is speeded up to a degree, thus showing an advanced peak in the heat flow results. When the hydrolyzation of silane is finished, the formed silanol monomers and multimers coming from polymerization tend to approach the precursor particles and be adsorbed onto the surface due to the coupling effect [44]. It is believed that the coupling sites are closely correlated with the hydroxyl groups attached to the silicon and aluminum superficially [77]. In view of the higher content of the two elements in fly ash than that in slag, it can be deduced that there are more coupling sites located at the surface of fly ash grains than slag grains for the same exposed surface area. As for the same particles with different size, larger particles are thought to possess more sites because of the larger superficial area. The coupled silanol monomers can prevent the free transport of water and various ions, thus retarding the hydration process in a way, as observed in the XRD, FTIR, thermogravimetry, compressive strength, pore structure and XPS results. On account of the quantitative difference of coupling sites between the two precursors, the hydration of fly ash experiences stronger inhibition effect, so the corresponding gel product, namely N-A-S-H type gel has a lower proportion in the entirety, which has been confirmed by the FTIR and EDX data. Along with the massive formation of hydration products, the hydrolyzed silane is adsorbed on their surface by the action of hydrogen bond at first and ultimately the combination will be quite stable by forming the Si-O-T bonds. In fact, this process can be accelerated due to the inherent self-desiccation during the geopolymerization [78]. This reliable combination, as verified by the FTIR and XPS results, can hold for a long time of weathering and thus the modified geopolymer matrices have enduring and credible efficacies.

4.2. Contact angle evolution mode

Contact angle is the most important index when evaluating the hydrophobic property of modified cement-based or geopolymer-based materials for the need to acquire better durability [10,12,20,29]. However, the presented contact angle results in the literatures show distinct discrepancy in terms of the mode of evolution [12,28,44], and a reasonable explanation is not available yet. In this study, different variation tendencies of contact angle as the modulus changes are also observed, as demonstrated in Fig. 11. Here, the evolution pattern of the measured contact angle results is discussed combining with the theories of surface physical chemistry to obtain a more essential understanding.

The ordinary geopolymer matrices are hydrophilic with very low contact angles, resembling the cement-based materials [29]. It could be closely associated with the high surface free energy of the geopolymer surface [23]. According to the wettability theory presented by Young [79], the formed contact angle of water in the three-phase boundary is to behave as a low value for not violating the principle of minimum Gibbs free energy in the case of high-energy solid surface. As a certain content of silane is introduced into the geopolymer system, the hydrolyzed silane molecules will be adsorbed onto the surface of the reaction products by the coupling sites, which ultimately form firm chemical bonding. The alkyl groups of the silane molecules are deemed to constitute equal distribution over the surface of matrix, which convert the corresponding hydrophilic regions to hydrophobic regions by the coverage with silane of low surface energy. Under the circumstances, the surface is no longer single-phase and can be regarded as a composite consisting of gels and silane. For the composite surface, the measured contact angle is together determined by the properties of the two constituent materials, including the area ratios and surface free energies, referring to the Cassie–Baxter theory [69]. Consequently, the surface of the modified geopolymer as a whole becomes less hydrophilic, which can be confirmed by the increased contact angle.

It is noteworthy that the above discussion is based on the hypotheses of ideal conditions, including the flat surface and the absence of defects like voids and pores. The surface roughness has a significant impact over the contact angle results as demonstrated by Wenzel [79], which depends on the original wettability property of concerned surface. This is also an effective and prevailing method to fabricate super-hydrophobic surfaces with contact angle exceeding 150° as well as slight degree of hysteresis [80]. Nevertheless, the influence of surface roughness may not be taken into account here, because the measured surface possesses originally certain smoothness and has experienced the polishing process, deemed and found to have a negligible surface roughness level [12,29]. The presence of pore structure is a universal characteristic of geopolymer or cement based materials, which can influence the contact angle by changing the fractional contact of water/air interface based on the theory of Cassie–Baxter [69]. Generally, a higher porosity means more area of the water/air interface and higher contact angle. However, for low silane dosages, the change of porosity is relatively non-significant as shown in Section 3.3, compared to the direct decrease of surface free energy induced by adding silane, and thus the influence of the latter on contact angle is dominant at this stage. When a greater amount of silane is applied, the superficial density of the alkyl groups increases accordingly, and hence the lower-energy matrix surface is obtained, showing stronger hydrophobicity. However, the coupling sites on the hydration gels are finite and if they are occupied completely, a larger dosage is thought to only aggrandize the thickness of the silane molecular layer [81] and thus lessen the porosity of substrate, as evidenced by the MIP results in Fig. 10. Under the circumstances, the distribution density of alkyl groups is not really aggrandized, which makes no contribution to the increase of hydrophobization effect. Combining with the influences of solid surface energy and porosity, the reduction of contact angle after reaching a maximum is expected. This is exactly the evolution process of measured contact angle for modulus 1.5, as presented in Fig. 11. For moduli 1.75 and 2, due to their greater porosities and accordingly more surface area, it takes more silane to cover the surface to achieve the maximum superficial density of alkyl groups than the case of modulus 1.5. It is believed that the needed dosages of silane to obtain the maximal contact angles for moduli 1.75 and 2 are beyond the dosage range adopted in this study, and thus the reduction of contact angle belonging to a part of the evolution process is not observed.

Considering the above-mentioned discussion, a theoretical formula applied to describe the evolution of contact angle for the geopolymer matrix modified by silane is derived in this study. At first, the Cassie–Baxter model which is appropriate for substrate constituted by two components is here adopted [82], and the contact angle θ^* on the substrate is expressed as,

$$\cos\theta^* = f_1 \cos\theta_1 + f_2 \cos\theta_2 \tag{3}$$

where f_1 and f_2 represent the water/solid contact region percentages of substrate constituents 1 and 2 respectively, θ_1 and θ_2 refer to contact angles of water over the intact surface of the two pure constituents, and $f_1 + f_2 = 1$. The surface of geopolymer matrices modified by silane can be seen as a two-constituents material with the region percentage of silane denoted by α hereafter, and the following equation is obtained as,

$$\cos\theta^* = 1 - \alpha(1 - \cos\theta_s) \tag{4}$$

where θ_s is the contact angle of water over the pure silane and the contact angle corresponding to the constituent of solid matrices can be deemed as 0 due to the inherent hydrophilic characteristic [83].

Next, the impact of pore structure is taken into account and the corresponding expression of the actually measured contact angle θ is written as follows,

$$\cos\theta = (1-\rho)\cos\theta^{*} - \rho \tag{5}$$

where ρ is the porosity of the geopolymer substrate. Ultimately, the desired formula can be gained by combining with equations (4) and (5), expressed as,

$$\cos\theta = (1-\rho)[2-\alpha(1-\cos\theta_s)] - 1 \text{ or } \theta = \arccos\{(1-\rho)[2-\alpha(1-\cos\theta_s)] - 1\} \tag{6}$$

To better understand this equation, the representative curves are obtained by assigning appropriate values to the variables, as presented in Fig. 16. The θ_s was reported to be about 110° [84] and is set as 100 or 110° here to find out its influence, with the angle identified from the number at the end of the legend. Different porosities are adopted to approach the characteristic of the measured samples, denoted as LowP, MediumP and HighP respectively. It can be found that the curves are well related to the variation tendency of contact angle results, demonstrating the rationality of the proposed formula. Moreover, the curves seem to give better description of the results at higher silane content than that of low silane dosage. This is because the geopolymer substrate is an absorbing medium, which means that continuous imbibition of water may happen during the contact angle measurement. Therefore the equilibrium contact angle is difficult to obtain and the measured angle could be greatly reduced [85]. This vast discrepancy caused by capillary absorption is to be quite negligible when the imbibition is suppressed, as observed in the high silane content range with better hydrophobicity. Furthermore, the θ_s value is seen to only change the quantity to certain degree without influencing the tendency of curves, which represents the effects of various waterproof agents. This equation can be an attempt to design the hydrophobic performance of the final geopolymer products on demand. Due to the great impact of contact angle over the water imbibition behavior as reflected in Fig. 12, it is expected to help to produce matrix having a low water absorption with an appropriate dosage of silane potentially. However, considering that the substrate interspace is controlled by the complex interaction between added silane and the hardened product, it is difficult to obtain a straightforward expression of full description of the changed porosity. Moreover, the area percentage of silane is influenced not only by the its quantity but also the total superficial area of hydration products with the limitation imposed by the distribution of coupling sites. With all these factors to be determined precisely, there are still more relevant efforts needed to be made before the suggested equation can be directly used in the industrial production.

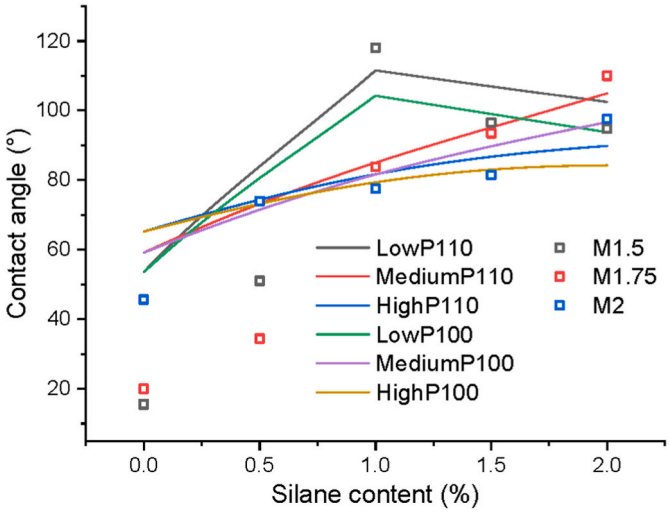

Fig. 16. The representative curves drawn according to equation (6).

5. Conclusions

This study comprehensively investigates the hydrophobicity properties and reaction products of FSBG pastes modified by a silane admixture. The underlying hydrophobic mechanism and the contact angle evolution are discussed in detail on the basis of integrated microscopic characterizations of the gel products with the hydration kinetics. The main conclusions can be made as follows:

- The coexistence of C-A-S-H and N-A-S-H gels is confirmed in the FSBG system according to the FTIR and EDX data. However, the formation of N-A-S-H gel is found to be restrained more intensely in the two gels with the use of silane, which is correlated with the higher amount of coupling sites located at the surface of fly ash particles and thus more silane adsorption.
- The addition of silane can effectively improve the erosion resistance of FSBG matrix with enabled hydrophobicity and lowered water absorption. Nevertheless, the mechanical strength in the long term is compromised. The increase of activator modulus has a negative impact over the strength and capillary absorption due to the higher porosity for the moduli range adopted in current research.
- The early compressive strength of FSBG at 1 day is found to slightly increase by introducing silane, which is consistent with the observed heat flow results. This can be mainly ascribed to the heat release along with the hydrolysis of silane, which completes within few hours after the mixing process and thus has a negligible effect for longer ages.
- With the application of silane, the reduction in porosity can be observed despite that the formation of hydration products is suppressed meanwhile, revealed from the FTIR, XRD and thermogravimetry results at 28 days. It may originate from the silane molecular layer occupying certain pore space, which is considered not to be incorporated into the gel skeleton and thus has less influence on the strength. This is why the porosity is actually not in accordance with the mechanical property.
- The evolution of contact angle on the surface of FSBG modified by silane is found to be closely dependent on its amount or more specifically its superficial density. However, the density has a maximum value caused by the restricted coupling sites, and thus excessive silane would not help but even worsen the hydrophobicity of the surface due to the reduced porosity.
- The contact angle evolution mode is revealed by proposing a formula, which can help to regulate and control the hydrophobicity properties of FSBG potentially. Moreover, due to the universal prerequisites adopted during the argumentation, they are also expected to be applicable for other geopolymer systems or cement-based materials with modification.

Declaration of competing interest

The authors declare that they have no known competing financial interests or personal relationships that could have appeared to influence the work reported in this paper.

Data availability

Data will be made available on request.

Acknowledgment

This work was financially supported by the National Natural Science Foundation of China (Grant No. 52178246; 52203381) and Postdoctoral Research Foundation of China (Grant No. 2022M712475).

References

[1] J.L. Provis, A. Palomo, C. Shi, Advances in understanding alkali-activated materials, Cement Concr. Res. 78 (2015) 110–125, https://doi.org/10.1016/j.cemconres.2015.04.013.

[2] C. Shi, B. Qu, J.L. Provis, Recent progress in low-carbon binders, Cement Concr. Res. 122 (2019) 227–250.

[3] Z. Zhang, J.L. Provis, A. Reid, H. Wang, Fly ash-based geopolymers: the relationship between composition, pore structure and efflorescence, Cement Concr. Res. 64 (2014) 30–41, https://doi.org/10.1016/j.cemconres.2014.06.004.

[4] P. Duxson, J.L. Provis, G.C. Lukey, J.S.J. van Deventer, The role of inorganic polymer technology in the development of 'green concrete, Cement Concr. Res. 37 (2007) 1590–1597, https://doi.org/10.1016/j.cemconres.2007.08.018.

[5] X. Gao, Q.L. Yu, A. Lazaro, H.J.H. Brouwers, Investigation on a green olivine nano-silica source based activator in alkali activated slag-fly ash blends: reaction kinetics, gel structure and carbon footprint, Cement Concr. Res. 100 (2017) 129–139, https://doi.org/10.1016/j.cemconres.2017.06.007.

[6] C. Li, H. Sun, L. Li, A review: the comparison between alkali-activated slag (Si+Ca) and metakaolin (Si+Al) cements, Cement Concr. Res. 40 (2010) 1341–1349, https://doi.org/10.1016/j.cemconres.2010.03.020.

[7] S. Puligilla, P. Mondal, Role of slag in microstructural development and hardening of fly ash-slag geopolymer, Cement Concr. Res. 43 (2013) 70–80, https://doi.org/10.1016/j.cemconres.2012.10.004.

[8] Y. Luo, S.H. Li, K.M. Klima, H.J.H. Brouwers, Q. Yu, Degradation mechanism of hybrid fly ash/slag based geopolymers exposed to elevated temperatures, Cement Concr. Res. 151 (2022), https://doi.org/10.1016/j.cemconres.2021.106649.

[9] S. Zhang, A. Keulen, K. Arbi, G. Ye, Waste glass as partial mineral precursor in alkali-activated slag/fly ash system, Cement Concr. Res. 102 (2017) 29–40, https://doi.org/10.1016/j.cemconres.2017.08.012.

[10] Q. Li, K. Yang, C. Yang, An alternative admixture to reduce sorptivity of alkali-activated slag cement by optimising pore structure and introducing hydrophobic film, Cem. Concr. Compos. 95 (2019) 183–192.

[11] C. Hall, Capillary imbibition in cement-based materials with time-dependent permeability, Cement Concr. Res. 124 (2019), https://doi.org/10.1016/j.cemconres.2019.105835.

[12] C. Zhang, S. Zhang, J. Yu, X. Kong, Water absorption behavior of hydrophobized concrete using silane emulsion as admixture, Cement Concr. Res. 154 (2022), 106738, https://doi.org/10.1016/j.cemconres.2022.106738.

[13] S.A. Bernal, R. Mejía de Gutiérrez, A.L. Pedraza, J.L. Provis, E.D. Rodriguez, S. Delvasto, Effect of binder content on the performance of alkali-activated slag concretes, Cement Concr. Res. 41 (2011) 1–8, https://doi.org/10.1016/j.cemconres.2010.08.017.

[14] M. Rostami, K. Behfarnia, The effect of silica fume on durability of alkali activated slag concrete, Construct. Build. Mater. 134 (2017) 262–268, https://doi.org/10.1016/j.conbuildmat.2016.12.072.

[15] S. Bernal, R. De Gutierrez, S. Delvasto, E. Rodriguez, Performance of an alkali-activated slag concrete reinforced with steel fibers, Construct. Build. Mater. 24 (2010) 208–214, https://doi.org/10.1016/j.conbuildmat.2007.10.027.

[16] P.S. Deb, P.K. Sarker, S. Barbhuiya, Sorptivity and acid resistance of ambient-cured geopolymer mortars containing nano-silica, Cem. Concr. Compos. 72 (2016) 235–245, https://doi.org/10.1016/j.cemconcomp.2016.06.017.

[17] C. Chaicharn, C. Prinya, S. Vanchai, R. Sumrerng, S. Apha, High-calcium bottom ash geopolymer: sorptivity, pore size, and resistance to sodium sulfate attack, J. Mater. Civ. Eng. 25 (2013) 105–111, https://doi.org/10.1061/(ASCE)MT.1943-5533.0000560.

[18] Z. Feng, F. Wang, T. Xie, J. Ou, M. Xue, W. Li, Integral hydrophobic concrete without using silane, Construct. Build. Mater. 227 (2019), 116678, https://doi.org/10.1016/j.conbuildmat.2019.116678.

[19] H.Y. Moon, D.G. Shin, D.S. Choi, Evaluation of the durability of mortar and concrete applied with inorganic coating material and surface treatment system, Construct. Build. Mater. 21 (2007) 362–369, https://doi.org/10.1016/j.conbuildmat.2005.08.012.

[20] F. Wang, S. Lei, J. Ou, W. Li, Effect of PDMS on the waterproofing performance and corrosion resistance of cement mortar, Appl. Surf. Sci. 507 (2020), https://doi.org/10.1016/j.apsusc.2019.145016.

[21] Z. Qu, S. Guo, Y. Zheng, E.C. Giakoumatos, Q. Yu, I.K. Voets, A simple method to create hydrophobic mortar using bacteria grown in liquid cultures, Construct. Build. Mater. 297 (2021), 123744, https://doi.org/10.1016/j.conbuildmat.2021.123744.

[22] H.S. Wong, R. Barakat, A. Alhilali, M. Saleh, C.R. Cheeseman, Hydrophobic concrete using waste paper sludge ash, Cement Concr. Res. 70 (2015) 9–20, https://doi.org/10.1016/j.cemconres.2015.01.005.

[23] J. Zhao, X. Gao, S. Chen, H. Lin, Z. Li, X. Lin, Hydrophobic or superhydrophobic modification of cement-based materials: a systematic review, Compos. B Eng. 243 (2022), 110104, https://doi.org/10.1016/j.compositesb.2022.110104.

[24] R. Di Mundo, C. Labianca, G. Carbone, M. Notarnicola, Recent advances in hydrophobic and icephobic surface treatments of concrete, Coatings 10 (2020), https://doi.org/10.3390/COATINGS10050449.

[25] Y.G. Zhu, S.C. Kou, C.S. Poon, J.G. Dai, Q.Y. Li, Influence of silane-based water repellent on the durability properties of recycled aggregate concrete, Cem. Concr. Compos. 35 (2013) 32–38, https://doi.org/10.1016/j.cemconcomp.2012.08.008.

[26] Y. Wu, L. Dong, X. Shu, Y. Yang, W. She, Q. Ran, A review on recent advances in the fabrication and evaluation of superhydrophobic concrete, Compos. B Eng. (2022), 109867.

[27] D. Zhang, H. Zhu, Q. Wu, T. Yang, Z. Yin, L. Tian, Investigation of the hydrophobicity and microstructure of fly ash-slag geopolymer modified by polydimethylsiloxane, Construct. Build. Mater. 369 (2023), 130540, https://doi.org/10.1016/j.conbuildmat.2023.130540.

[28] B. Feng, J. Liu, Y. Chen, X. Tan, M. Zhang, Z. Sun, Properties and microstructure of self-waterproof metakaolin geopolymer with silane coupling agents, Construct. Build. Mater. 342 (2022), 128045, https://doi.org/10.1016/j.conbuildmat.2022.128045.

[29] S. Ruan, D. Yan, S. Chen, F. Jiang, W. Shi, Process and mechanisms of multi-stage water sorptivity in hydrophobic geopolymers incorporating polydimethylsiloxane, Cem. Concr. Compos. 128 (2022), 104460, https://doi.org/10.1016/j.cemconcomp.2022.104460.

[30] S. Ruan, S. Chen, J. Lu, Q. Zeng, Y. Liu, D. Yan, Waterproof geopolymer composites modified by hydrophobic particles and polydimethylsiloxane, Compos. B Eng. 237 (2022), 109865, https://doi.org/10.1016/j.compositesb.2022.109865.

[31] X. Xue, Y.-L. Liu, J.-G. Dai, C.-S. Poon, W.-D. Zhang, P. Zhang, Inhibiting efflorescence formation on fly ash–based geopolymer via silane surface modification, Cem. Concr. Compos. 94 (2018) 43–52, https://doi.org/10.1016/j.cemconcomp.2018.08.013.

[32] GB/T, Method of testing cements-Determination of strength, in: China Natiaonal Stand, 1999, 17671-1999.

[33] ASTM C642-06, Standard test method for density, Absorption, and Voids in Hardened Concrete, ASTM Int., 2006.

[34] ASTM C1585-13, Standard Test Method for Measurement of Rate of Absorption of Water by Hydraulic Cement Concretes, ASTM Int., 2013.

[35] A.R. Brough, A. Atkinson, Sodium silicate-based, alkali-activated slag mortars: Part I. Strength, hydration and microstructure, Cement Concr. Res. 32 (2002) 865–879, https://doi.org/10.1016/S0008-8846(02)00717-2.

[36] Y. Zuo, M. Nedeljković, G. Ye, Coupled thermodynamic modelling and experimental study of sodium hydroxide activated slag, Construct. Build. Mater. 188 (2018) 262–279, https://doi.org/10.1016/j.conbuildmat.2018.08.087.

[37] A. Fernández-Jiménez, F. Puertas, Setting of alkali-activated slag cement. Influence of activator nature, Adv. Cement Res. 13 (2001) 115–121, https://doi.org/10.1680/adcr.2001.13.3.115.

[38] K. Sagoe-Crentsil, L. Weng, Dissolution processes, hydrolysis and condensation reactions during geopolymer synthesis: Part II. High Si/Al ratio systems, J. Mater. Sci. 42 (2007) 3007–3014, https://doi.org/10.1007/s10853-006-0818-9.

[39] M. Criado, A. Fernández-Jiménez, A. Palomo, I. Sobrados, J. Sanz, Effect of the SiO2/Na2O ratio on the alkali activation of fly ash. Part II: 29Si MAS-NMR Survey, Microporous Mesoporous Mater. 109 (2008) 525–534, https://doi.org/10.1016/j.micromeso.2007.05.062.

[40] S. Saeed, R.M. Al Soubaihi, L.S. White, M.F. Bertino, K.M. Saoud, Rapid fabrication of cross-linked silica aerogel by laser induced gelation, Microporous Mesoporous Mater. 221 (2016) 245–252, https://doi.org/10.1016/j.micromeso.2015.09.012.

[41] K. Tosun, B. Felekoglu, B. Baradan, Effectiveness of alkyl alkoxy silane treatment in mitigating alkali-silica reaction, ACI Mater. J. 105 (2008) 20–27. https://www.proquest.com/scholarly-journals/effectiveness-alkyl-alkoxy-silane-treatment/docview/198104743/se-2?accountid=15157.

[42] L.E. Prevette, T.E. Kodger, T.M. Reineke, M.L. Lynch, Deciphering the role of hydrogen bonding in enhancing pDNA−Polycation interactions, Langmuir 23 (2007) 9773–9784, https://doi.org/10.1021/la7009995.

[43] B. Chen, H. Shao, B. Li, Z. Li, Influence of silane on hydration characteristics and mechanical properties of cement paste, Cem. Concr. Compos. 113 (2020), 103743, https://doi.org/10.1016/j.cemconcomp.2020.103743.

[44] J. Yang, W. She, W. Zuo, K. lyu, Q. Zhang, Rational application of nano-SiO2 in cement paste incorporated with silane: counterbalancing and synergistic effects, Cem. Concr. Compos. 118 (2021), 103959, https://doi.org/10.1016/j.cemconcomp.2021.103959.

[45] Z. Sun, A. Vollpracht, Isothermal calorimetry and in-situ XRD study of the NaOH activated fly ash, metakaolin and slag, Cement Concr. Res. 103 (2018) 110–122, https://doi.org/10.1016/j.cemconres.2017.10.004.

[46] S.A. Bernal, J.L. Provis, B. Walkley, R. San Nicolas, J.D. Gehman, D.G. Brice, A. R. Kilcullen, P. Duxson, J.S.J. van Deventer, Gel nanostructure in alkali-activated binders based on slag and fly ash, and effects of accelerated carbonation, Cement Concr. Res. 53 (2013) 127–144, https://doi.org/10.1016/j.cemconres.2013.06.007.

[47] T.A. Aiken, J. Kwasny, W. Sha, M.N. Soutsos, Effect of slag content and activator dosage on the resistance of fly ash geopolymer binders to sulfuric acid attack, Cement Concr. Res. 111 (2018) 23–40, https://doi.org/10.1016/j.cemconres.2018.06.011.

[48] A. Rafeet, R. Vinai, M. Soutsos, W. Sha, Effects of slag substitution on physical and mechanical properties of fly ash-based alkali activated binders (AABs), Cem, Concr. Res. 122 (2019) 118–135, https://doi.org/10.1016/j.cemconres.2019.05.003.

[49] S.-D. Wang, K.L. Scrivener, Hydration products of alkali activated slag cement, Cement Concr. Res. 25 (1995) 561–571, https://doi.org/10.1016/0008-8846(95)00045-E.

[50] O. Burciaga-Díaz, J.I. Escalante-García, Structure, mechanisms of reaction, and strength of an alkali-activated blast-furnace slag, J. Am. Ceram. Soc. 96 (2013) 3939–3948, https://doi.org/10.1111/jace.12620.

[51] C. Zhang, S. Lu, Z. Zhang, M. Zhong, Y. Li, X. Huang, W. Xu, D. Wang, L. Wang, The effect of phosphorus on the formation of mullite whiskers from citric acid activated kaolin, Ceram. Int. 44 (2018) 18796–18802, https://doi.org/10.1016/j.ceramint.2018.07.112.

[52] J.M. Gallardo Amores, V. Sanchez Escribano, G. Busca, Characterisation of Fe–Cr–Al mixed oxides, Mater. Chem. Phys. 60 (1999) 168–176, https://doi.org/10.1016/S0254-0584(99)00056-5.

[53] F.B. Reig, J.V.G. Adelantado, M.C.M. Moya Moreno, FTIR quantitative analysis of calcium carbonate (calcite) and silica (quartz) mixtures using the constant ratio

method. Application to geological samples, Talanta 58 (2002) 811–821, https://doi.org/10.1016/S0039-9140(02)00372-7.
[54] N. V Chukanov, A.D. Chervonnyi, Infrared Spectroscopy of Minerals and Related Compounds, Springer, 2016.
[55] I. Ismail, S.A. Bernal, J.L. Provis, R. San Nicolas, S. Hamdan, J.S.J. van Deventer, Modification of phase evolution in alkali-activated blast furnace slag by the incorporation of fly ash, Cem. Concr. Compos. 45 (2014) 125–135, https://doi.org/10.1016/j.cemconcomp.2013.09.006.
[56] S. Zhang, Z. Li, B. Ghiassi, S. Yin, G. Ye, Fracture properties and microstructure formation of hardened alkali-activated slag/fly ash pastes, Cement Concr. Res. 144 (2021), 106447, https://doi.org/10.1016/j.cemconres.2021.106447.
[57] W.K.W. Lee, J.S.J. van Deventer, Use of infrared spectroscopy to study geopolymerization of heterogeneous amorphous aluminosilicates, Langmuir 19 (2003) 8726–8734, https://doi.org/10.1021/la026127e.
[58] M.B. Toffolo, L. Regev, S. Dubernet, Y. Lefrais, E. Boaretto, FTIR-based crystallinity assessment of aragonite–calcite mixtures in archaeological lime binders altered by diagenesis, Minerals 9 (2019), https://doi.org/10.3390/min9020121.
[59] N. Li, N. Farzadnia, C. Shi, Microstructural changes in alkali-activated slag mortars induced by accelerated carbonation, Cem, Concr. Res. 100 (2017) 214–226, https://doi.org/10.1016/j.cemconres.2017.07.008.
[60] P. Liu, J. Song, L. He, X. Liang, H. Ding, Q. Li, Alkoxysilane functionalized polycaprolactone/polysiloxane modified epoxy resin through sol–gel process, Eur. Polym. J. 44 (2008) 940–951, https://doi.org/10.1016/j.eurpolymj.2007.12.014.
[61] H. Li, Y. Liu, K. Yang, C. Liu, X. Guan, S. Liu, G. Jing, Effects of synthetic CSH-tartaric acid nanocomposites on the properties of ordinary Portland cement, Cem. Concr. Compos. 129 (2022), 104466, https://doi.org/10.1016/j.cemconcomp.2022.104466.
[62] Z. Li, T. Lu, X. Liang, H. Dong, G. Ye, Mechanisms of autogenous shrinkage of alkali-activated slag and fly ash pastes, Cement Concr. Res. 135 (2020), 106107, https://doi.org/10.1016/j.cemconres.2020.106107.
[63] I. Garcia-Lodeiro, A. Palomo, A. Fernández-Jiménez, D.E. Macphee, Compatibility studies between N-A-S-H and C-A-S-H gels. Study in the ternary diagram Na2O–CaO–Al2O3–SiO2–H2O, Cement Concr. Res. 41 (2011) 923–931, https://doi.org/10.1016/j.cemconres.2011.05.006.
[64] A. Aboulayt, F. Souayfan, E. Roziere, R. Jaafri, A. Cherki El Idrissi, R. Moussa, C. Justino, A. Loukili, Alkali-activated grouts based on slag-fly ash mixtures: from early-age characterization to long-term phase composition, Construct. Build. Mater. 260 (2020), 120510, https://doi.org/10.1016/j.conbuildmat.2020.120510.
[65] M. Xie, Y. Zhong, Z. Li, F. Lei, Z. Jiang, Study on alkylsilane-incorporated cement composites: hydration mechanism and mechanical properties effects, Cem. Concr. Compos. 122 (2021), 104161, https://doi.org/10.1016/j.cemconcomp.2021.104161.
[66] Z.Y. Qu, Q. Yu, Y.D. Ji, F. Gauvin, I.K. Voets, Mitigating shrinkage of alkali activated slag with biofilm, Cement Concr. Res. 138 (2020), 106234, https://doi.org/10.1016/j.cemconres.2020.106234.
[67] K.K. Aligizaki, Pore Structure of Cement-Based Materials: Testing, Interpretation and Requirements, Crc Press, 2005.
[68] W. Werner, I. Halász, Pore structure of chemically modified silica gels determined by exclusion chromatography, J. Chromatogr. Sci. 18 (1980) 277–283, https://doi.org/10.1093/chromsci/18.6.277.
[69] A.B.D. Cassie, S. Baxter, Wettability of porous surfaces, Trans. Faraday Soc. 40 (1944) 546–551.
[70] C.-H. Lee, W.-C. Chen, Y.L. Khung, XPS analysis of 2- and 3-aminothiophenol grafted on silicon (111) hydride surfaces, Molecules 23 (2018), https://doi.org/10.3390/molecules23102712.
[71] M. Makehelwala, Y. Wei, S.K. Weragoda, R. Weerasooriya, Ca2+ and SO42− interactions with dissolved organic matter: implications of groundwater quality for CKDu incidence in Sri Lanka, J. Environ. Sci. 88 (2020) 326–337, https://doi.org/10.1016/j.jes.2019.09.018.
[72] J. Zhou, F. Li, C. Du, J. Liu, Y. Wang, W. Li, G. He, Q. He, Photodegradation performance and recyclability of a porous nitrogen and carbon co-doped TiO 2/activated carbon composite prepared by an extremely fast one-step microwave method, RSC Adv. 6 (2016) 84457–84463.
[73] H. Herb, A. Gerdes, G. Brenner-Weiß, Characterization of silane-based hydrophobic admixtures in concrete using TOF-MS, Cement Concr. Res. 70 (2015) 77–82, https://doi.org/10.1016/j.cemconres.2015.01.008.
[74] L.M. Kljajević, S.S. Nenadović, M.T. Nenadović, N.K. Bundaleski, B.Ž. Todorović, V. B. Pavlović, Z.L. Rakočević, Structural and chemical properties of thermally treated geopolymer samples, Ceram. Int. 43 (2017) 6700–6708, https://doi.org/10.1016/j.ceramint.2017.02.066.
[75] E. John, J.D. Epping, D. Stephan, The influence of the chemical and physical properties of C-S-H seeds on their potential to accelerate cement hydration, Construct. Build. Mater. 228 (2019), 116723, https://doi.org/10.1016/j.conbuildmat.2019.116723.
[76] M.D. Andersen, H.J. Jakobsen, J. Skibsted, Characterization of white Portland cement hydration and the C-S-H structure in the presence of sodium aluminate by 27Al and 29Si MAS NMR spectroscopy, Cement Concr. Res. 34 (2004) 857–868, https://doi.org/10.1016/j.cemconres.2003.10.009.
[77] J.L. Zimmermann, T. Nicolaus, G. Neuert, K. Blank, Thiol-based, site-specific and covalent immobilization of biomolecules for single-molecule experiments, Nat. Protoc. 5 (2010) 975–985.
[78] Z. Li, M. Nedeljković, B. Chen, G. Ye, Mitigating the autogenous shrinkage of alkali-activated slag by metakaolin, Cem, Concr. Res. 122 (2019) 30–41, https://doi.org/10.1016/j.cemconres.2019.04.016.
[79] B. Bhushan, Y.C. Jung, Natural and biomimetic artificial surfaces for superhydrophobicity, self-cleaning, low adhesion, and drag reduction, Prog. Mater. Sci. 56 (2011) 1–108, https://doi.org/10.1016/j.pmatsci.2010.04.003.
[80] D. Wang, Q. Sun, M.J. Hokkanen, C. Zhang, F.-Y. Lin, Q. Liu, S.-P. Zhu, T. Zhou, Q. Chang, B. He, Q. Zhou, L. Chen, Z. Wang, R.H.A. Ras, X. Deng, Design of robust superhydrophobic surfaces, Nature 582 (2020) 55–59, https://doi.org/10.1038/s41586-020-2331-8.
[81] G. Xiong, B. Luo, X. Wu, G. Li, L. Chen, Influence of silane coupling agent on quality of interfacial transition zone between concrete substrate and repair materials, Cem. Concr. Compos. 28 (2006) 97–101, https://doi.org/10.1016/j.cemconcomp.2005.09.004.
[82] C.E. Cansoy, H.Y. Erbil, O. Akar, T. Akin, Effect of pattern size and geometry on the use of Cassie–Baxter equation for superhydrophobic surfaces, Colloids Surfaces A Physicochem. Eng. Asp. 386 (2011) 116–124, https://doi.org/10.1016/j.colsurfa.2011.07.005.
[83] H. Chen, M. Wyrzykowski, K. Scrivener, P. Lura, Prediction of self-desiccation in low water-to-cement ratio pastes based on pore structure evolution, Cem, Concr. Res. 49 (2013) 38–47, https://doi.org/10.1016/j.cemconres.2013.03.013.
[84] C. Erich Zybill, H. Ghee Ang, L. Lan, W. Ying Choy, E. Fang Kin Meng, Monomolecular silane films on glass surfaces—contact angle measurements, J. Organomet. Chem. 547 (1997) 167–172, https://doi.org/10.1016/S0022-328X(97)00205-2.
[85] S. Krainer, U. Hirn, Contact angle measurement on porous substrates: effect of liquid absorption and drop size, Colloids Surfaces A Physicochem. Eng. Asp. 619 (2021), 126503, https://doi.org/10.1016/j.colsurfa.2021.126503.